STUDY OF LARGE MOLECULAR WEIGHT POLY(ISOPRENE-B-STYRENE-B-ETHYLENE OXIDE) AND OF ITS HYBRID OXIDES AND NITRIDES

A Thesis

Presented to the Faculty of the Graduate School

of Cornell University

In Partial Fulfillment of the Requirements for the Degree of

Master of Science

By

Ji-yeob Kim

August 2014

ABSTRACT

In this study, poly(isoprene-block-styrene-block-ethylene oxide) (ISO) with molecular weight of 93,496 g mol^{-1} was synthesized to investigate the effect of large molecular weight on polymer phase behavior. This polymer was used to direct aluminosilicate hybrids and results compared with a 23,180 g mol^{-1} ISO-aluminosilicate hybrid system, i.e. with work of previous Wiesner group member, Juho Kim. Results showed that, despite the occurrence of more mixed phases with the larger ISO, both ISO-aluminosilicate hybrid systems display the same sequence of phases with those of the 93,496 g mol^{-1} ISO aluminosilicate hybrid structures shifted down to lower O + inorganic volume fractions as compared to the 23,180 g mol^{-1} ISO.

Subsequently, several other metal oxide hybrids derived from 93,496 g mol^{-1} ISO were studied. The goal of the study was, again to learn about the structure-directing behavior of large molecular weight polymer, and identify ways to obtain uniform phases. This is usually a challenge as a result of the much slower chain dynamics observed for large molecular weight polymer. Uniform structures from large polymers enable access to large pore and strut size mesoporous materials desirable for a numbers of applications. Titanium (IV) oxide and niobium(V) oxide hybrids were studied, which have been previously examined with smaller molecular weight ISO. Niobium (V) oxide can be further nitrided into niobium nitride, which has the potential to show superconductivity. The temperature- and time-dependence of nitriding were investigated to identify optimal conditions. Finally, mesoporous

gallium nitride was prepared, by nitriding 93,496 g mol^{-1} ISO-derived gallium (III) oxide hybrids, but further studies are needed to bring this part of work to full fruition.

BIOGRAPHICAL SKETCH

I was born in Kyunggido, and raised in Seoul, South Korea. I have always loved adventures, and having new experiences. For this reason, I travelled many countries, which opened my eyes to a new world where people had completely different living standards compared to where I am from. Some of the countries had better knowledge of saving energy and utilizing their available space. Other countries, however, were lacking transportation and clean water, because they were not supported with enough energy for living.

Throughout the school years, I participated as a member of an orchestra as a trumpet player, a member of a hand-bell club, and an accompanist in a jazz choir. At the same time, I started having great interests in Physics, Chemistry and Biology. Chilliwack Senior Secondary School (CSSS) provided many opportunities to participate in various experiments, which enhanced my curiosity for Science. After coming back to Korea, I continued studying Science, specializing in Physics and Chemistry at Sehwa Girls' High School. I decided to study Materials Science and Engineering at Hanyang University as my travelling experiences that triggered my passion for the Energy Sciences. At Hanyang University, I focused on the Physics of Materials, and worked as an intern at Nanoelectronics and Photonics Lab lead by Professor Won Il Park. Since 2012, I studied in polymer science and its inorganic hybrids, mesoporous oxides and nitride, in the Wiesner group lead by Professor Ulrich Wiesner, at the Materials Science and Engineering department of Cornell University.

김문규, 김경희, 김의태, 김다엽

ACKNOWLEDGMENTS

I would like to thank Professor Ulrich Wiesner, and Professor Francis J. DiSalvo for giving me an amazing opportunity to conduct research at Cornell University, with all their support. I would also like to thank Professor Christopher Umbach for showing great support and providing advice for my work and my future plans. My colleagues of the Wiesner group, especially Kwan W. Tan, Spencer Robbins, and Hiroaki Sai shared many valuable discussions with me and assisted me in pushing the research forward. Lastly, Cornell Center of Materials Research (CCMR), and Cornell High Energy Synchrotron Source (CHESS) supported this work.

Table of Contents

Chapter 1.

Introduction

As worldwide energy use increases, there is a growing need for renewable energy sources. Some examples of such renewable energy sources include: wind energy, water energy, nuclear energy and solar energy. Wind energy and water energy is not sufficient to meet the world's require units for energy, and the locations to generate energy are limited. Wind energy is also intermittent and generates power only when the wind blows. Nuclear energy has been studied and generated, and in fact, is one of the sources that supply huge portion of energy to many countries such as Germany, Turkey, France, India, and United States. However, nuclear energy generates radioactive matter, and as shown by the Fukushima Daiichi plant nuclear leak, in Japan, it has great potential to generate a disaster with fatal consequences for human and the ecosystem. For these reasons, solar energy has possibilities to become our next generation energy source, but it is not an exception in that there are still many issues to be dealt with. First, solar energy is obtainable only where there exists enough sunlight. For example, if there is not enough sunlight to generate energy, such as at night, or in cloudy or rainy weather, energy demand may not be met. This can be assisted by battery research for batteries can store energy as much as possible when sunlight is available to be used when sunlight is not available. Second, it is not easy to collect solar energy from sunlight even if there is enough of it. When sunlight meets the solar panel, the entirety of sunlight does not necessarily go into the panel, but some will reflect, scatter, or transfer into heat. The amount of sunlight absorption can be increased with various surface treatments.

To address some of the needs for next generation energy sources, nanotechnology can provide some advantages in energy systems. For example, providing nanostructured electrodes in batteries can decrease the solid state diffusion lengths in batteries, allowing for faster charge and discharge. Also for solar cells, having a nanostructure on the surface of solar panels could reduce reflection to help the panel absorb as much light as possible, or increase hydrophobicity so that it could prevent any dirt piling up on the panel that may compromise the sunlight absorption amount, and also could act as an electron/hole collector that is generated by the sunlight.

There are different ways to fabricate nanostructures. Conventionally, nanostructuring can be largely divided into two methods: top-down and bottom-up. In top-down methods, the desired nanostructure is obtained by repeatedly removing unwanted parts from bulk material. Examples of these methods are various lithography and nanocontact printing techniques. On the other hand, bottom-up methods grow nanostructure from a wafer by using atomic / molecular precursors to become the desired nanostructured material. This can be achieved by plasma arcing, chemical vapor deposition (CVD) and/or molecular beam epitaxy (MBE). These methods have been used in research and in industry widely, enabling production of one and two-dimensional structures such as nanofibers, nanoflowers, nanoparticles and nanorods. Sol-gel chemistry is another bottom-up method to build nanostructures. This, however, is differentiated from others in a way that it has potential to grow various complex three-dimensional materials via self-assembly. Also, it benefits from not requiring a wafer to grow from, and

extremely high temperature processes as often, for example, as CVD does. This opens access to materials not tolerant to high temperatures for which, therefore, producing nanostructures has been difficult.

Here, block copolymers, which will be introduced in Chapter 2, are used with several different inorganic materials to form various structures, including lamellar (LAM), alternating gyroid (Q214), double gyroid (Q230), and inverse hexagonal (HEX). Previously in the Wiesner group, small molecular mass diblock copolymers and triblock terpolymers, from 10,000 g/mol to 40,000 g/mol, were extensively studied. In the present, 93,500 g/mol poly(isoprene-b-styrene-b-ethylene oxide) (ISO) (Chapter 3) was synthesized and analyzed with gel permeation chromatography (GPC) and nuclear magnetic resonance (NMR), and was used to structure-direct inorganic materials including aluminosilicate (Chapter 4), titanium(IV) oxide, niobium(V) oxide, and gallium(III) oxide (Chapter 5). For the ISO-aluminosilicate part, its structures with different loading of O + oxide were examined, and were compared to a previous study with smaller molecular mass ISO (23,200 g/mol) to see if 93,500 g/mol molar mass polymers derived of materials follow the behavior of the 23,200 g/mol ISO based phase diagram. For titanium(IV) oxide, niobium(V) oxide, and gallium(III) oxide hybrids from 93,500 g/mol ISO, structure with varying inorganic content were studied, and nitrided at different temperatures. Morphologies were analyzed by small angle X-ray scattering (SAXS), transmission electron microscopy (TEM), and scanning electron microscopy (SEM) and their inorganic content was determined by thermogravimetric analysis (TGA), respectively.

Chapter 2.

Background

2.1 Block copolymer

A block copolymer is a macromolecule that consists two or more distinct polymer blocks. Due to their chemical incompatibility, they try to separate, but unlike oil and water, they fail to macrophase-separate because the blocks are connected. Instead, they would microphase-separate, and settle in a structure that is energetically favored, dictated by the degree of polymerization N , Flory-Huggins parameter χ , and volume fraction of block A, f_A . Bates and Fredrickson have calculated a diblock copolymer phase diagram as shown in Figure 1.

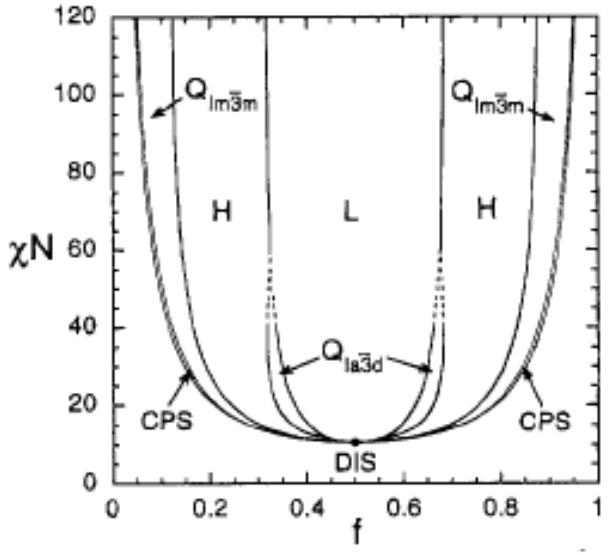

Figure 1. Diblock copolymer phase diagram suggested by G. H. Fredrickson[1]

Structures found in this system are body-centered cubic (Q_{Im3m}), gyorid(Q_{Ia3d}), lamellae (L), and hexagonally packed cylinders (H). Especially the gyroid

structure is interesting because it is a bicontinuous network structure. Diblock copolymer system provides gyroid structures, but only in narrow composition windows. More recently, triblock terpolymers have attracted attention because they provide larger composition windows for network structures. However, adding one more block increases the complexity by adding more substance parameters, and many studies have been performed to understand such systems.

2.2 Block Copolymer Hybrids

Polymers can be used as lithography mask and photonic materials due to their ability to form from distinct blocks of repeat units. However, they are composed of organic substances and thus limited in their properties relative, for example, to inorganic materials. When a block copolymer consists two or more blocks that are immiscible, like oil and water, they cannot macrophase-separate because they are covalently bonded together. Instead, different blocks will range to minimize enthalpy and entropy energy contributions, and therefore, self-assemble into unique structures. Functional materials can benefit from block copolymers' structure-directing ability when one can selectively dissolve them in one block, and form the final structure together. For example, nanoparticles could swell one of the blocks in a block copolymer and form particle rich domains to show functions of the nanoparticles[2]. In order to do this in bulk, one-pot type methods have been employed where they simply mix a block copolymer solution and

nanoparticle solution together. During drying at a certain temperature, the mixture undergoes evaporation-induced self-assembly to form a film, and the film product is called a *block copolymer hybrid*. Many block copolymer hybrids have been achieved with different inorganic materials, such as aluminosilicate[3], non-oxides[4], transition metal oxides[5], and metals[6].

Chapter 3.

Poly(isoprene-b-styrene-b-ethylene oxide) (ISO)

3.1 Motivation

Over several decades, many studies have been conducted to be able to predict AB diblock copolymer phase behavior[1], [7]–[10], and they are known to self-assemble into four structures: spheres, cylinders, lamellae, and gyroids. Their phase behavior is dictated by the degree of polymerization, N, the A block volume fraction, f_A, and the segment-segment interaction parameter, χ_{AB}. By adding one more block adds parameters, and ABC triblock terpolymers exhibit greater morphological complexity[11]–[18], which includes, for example, core-shell versions of structures found in diblock copolymer systems. On the other hand, this complexity provides potential for better control of mechanical properties [19].

Having one more block, ABC triblock terpolymers are much more complex than AB diblocks. Previously, structures generated in the ISO system with different volume fractions of each block have been studied, and many efforts were made to provide better understanding of the phase behavior, including attempts to assemble a phase diagram of the system[14][20]. The Wiesner group has been working to complete a phase diagram of ISO, blended with aluminosilicate nanoparticles. Here, a bigger molar mass ISO with 93,500 g mol^{-1} (JY06) was synthesized and its hybrid formation behavior compared with other molar mass ISO polymers.

3.2 Experimental Section

The synthesis of 23,200 g mol^{-1} ISO-1 and 93,500 g mol^{-1} JY06 are the same, except larger amounts of monomers were added to the synthesis, and the bigger polymer takes more time for the synthesis to be completed. The volume fractions of each block are summarized in Table 1.

Vol. fraction	PI	PS	PEO
JY06 (93,500 g mol^{-1})	0.34	0.60	0.06
ISO-1 (23,200 g mol^{-1})	0.31	0.52	0.17

Table 1. The volume fractions of each block in JY06 and ISO-1

In Figure 2, a schematic for the synthesis of ISO is shown. Most of the reaction was done in a glass vacuum line, and the glassware used for reactions were cleaned thoroughly with commercially provided tetrahydrofuran (THF) (Sigma-Aldrich, CAS No. 109-99-9), methanol (Sigma-Aldrich, CAS No. 67-56-1), and acetone (Sigma-Aldrich, CAS No. 67-64-1) in sequence, to mainly remove any organic material on the glassware, and subsequently dried with a heat gun at around 200˚C.

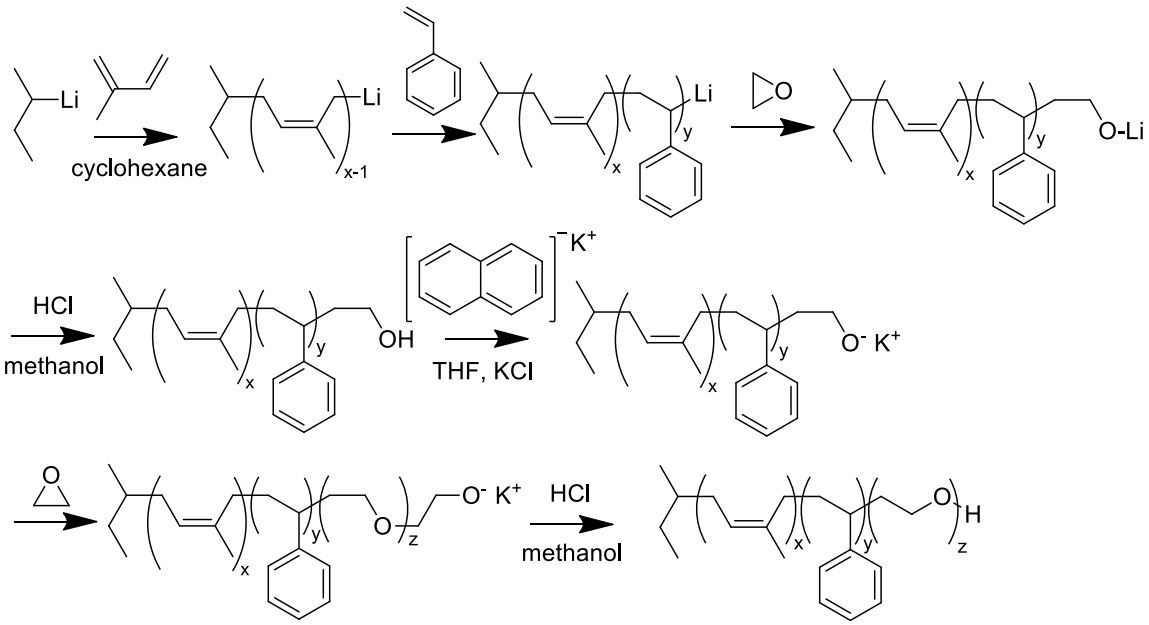

Figure 2. Schematic of poly(isoprene-b-styrene-b-ethylene oxide) synthesis

For the first block, isoprene, benzene was used as the solvent. In order to do this, commercially purchased benzene (Sigma-Aldrich, CAS No. 1076-43-3) was distilled in a vacuum line by freezing and pump-thawing three times. Freezing and pump-thawing means that a solution to be distilled was injected into a reactor at room temperature that is connected to, for example, to an ampoule by a glass-bridge. The ampoule is frozen by liquid nitrogen around 77 K. After vacuum is pulled onto the bridge, the reactor with the solution is opened for the solution to move to the ampoule due to the low pressure and the temperature difference between the reactor and the ampoule. Warm water may be applied to the outside reactor to help the benzene move to the ampoule. In the process, inhibitor and impurities from the original solution are removed, and the frozen solution in the

ampoule is expected to be pure. To make sure, this is thawed back to the solution state, and the processes are repeated three times.

On a vacuum line, a distillation bridge was set for isoprene distillation connecting a reactor and an ampoule. 25 mL of commercial isoprene (Sigma-Aldrich, CAS No. 78-79-5) was prepared at room temperature. First, n-butyllithium (Sigma-Aldrich, CAS No. 109-72-8) was injected into the reactor, and meanwhile, argon gas was flowing out of the reactor to prevent n-butyllithium from violently reacting with air. After the n-butyllithium had time to react with residual impurities, warmed up to room temperature isoprene was injected into the reactor and frozen and pump-thawed three times to be distilled and to remove any possible impurities and/or dissolved gas. The ampoule with the distilled isoprene was put into a metal can for thawing. The can is to minimize the impact in case of an explosion, since pure isoprene without inhibitor could be extremely reactive. The distilled isoprene and the distilled benzene in a separate vacuum-sealed sphere flasks were brought into glove box filled with inert gas (N_2 in this case) to prevent any contact with oxygen and/or water. The polymer initiator, sec-butyllithium (Sigma-Aldrich, CAS No. 598-31) was prepared at room temperature, 0.22 mL was brought out using a syringe with a needle, and it was also brought into the glove box. 7.75 g of distilled isoprene, and the 0.22mL sec-butyllithium were added to the distilled benzene mixture and stirred overnight.

On the same day isoprene was prepared, styrene (Sigma-Alrich CAS No. 100-42-5) was added to calcium hydride and stirred overnight in a distillation bridge, to

remove its inhibitor, and any water content. Reacting styrene with calcium hydride produces gas, and to prevent any pressurization, styrene was frozen and pump-thawed on the vacuum line. Meanwhile, ambient-temperature gel permeation chromatography (GPC) (Waters 410 differential refractive index detector) was used to analyze the polydispersity of the polyisoprene (PI). The GPC sample was made as followed. 2 mL of the solution of PI, sec-butyllithium, and benzene was taken out of the flask and 2 mL of methanol was added to terminate the PI. The solution turned cloudy upon termination. This solution was stirred vigorously and its solvent was poured out to leave the precipitate on the bottom. The precipitate was dried by rotary evaporation. Then, 1 to 2 mL of THF was added as the GPC uses THF as its solvent. The resulting polyisoprene showed a molecular mass of 29,800 g mol^{-1}, and a polydispersity index (PDI) of 1.03.

On the next day, styrene was frozen and pump-thawed three times to make sure it does not contain any impurities. The distilled styrene was vacuum-sealed and brought into the glove box and 15.1 g of it was added to the PI solution. The color of the solution changed into bright orange, which show that the PI block had reacted with styrene. This was stirred overnight and a GPC sample was prepared again with using same method introduced earlier for the PI and its PDI was 1.03.

The solution of poly(isoprene-b-styrene) (IS) was end-capped with ethylene oxide, then terminated with methanol, which is shown in Figure. 2. Especially the end-capping reaction can be seen in the second reaction, where ethylene oxide is added to the IS polymer that ends with a lithium ion. In order to add the next block

to the IS, in this case ethylene oxide, a bridge needs to form to connect the two, and this is achieved by adding one ethylene oxide unit to function as a bridge; this is called “end-capping” procedure. It is noted that in this experiment ethylene oxide is used for two different purposes: one, as the last block of the complete polymer ISO, and second, as a bridge reinitiated between the IS and O blocks of the polymers. The terminated polymer was then reinitiated by adding KN in THF and potassium chloride (KCl) (Mallinckrodt, CAS No. 7447-40-7), to initiate polymerization of the final block, ethylene oxide. This was, again, terminated with methanol and HCl, and the ISO was completed. This step is explained in more depth below.

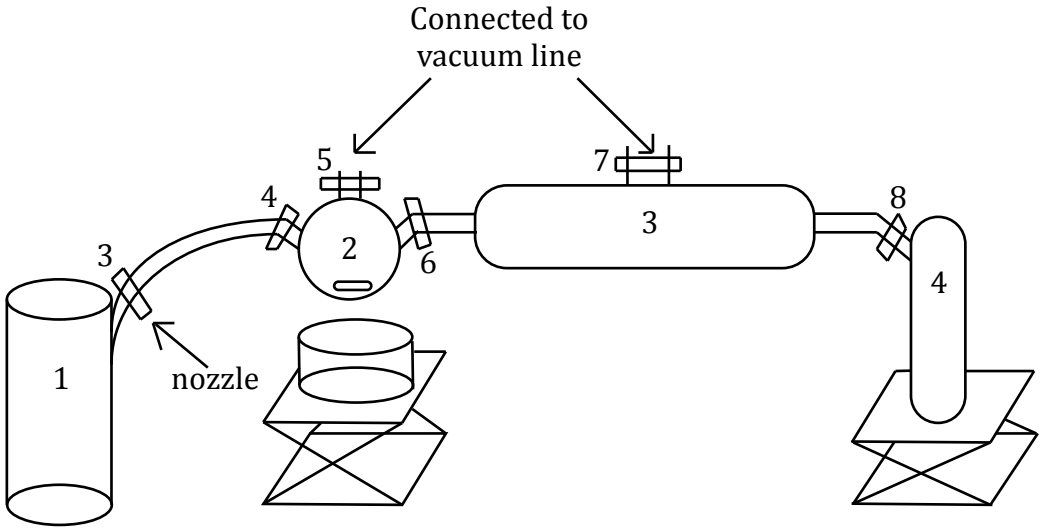

Figure 3. Schematic of ethylene oxide distillation set-up

Figure 3 depicts a simple version of the experimental setup for ethylene oxide distillation, in which every step is crucial and connected directly to safety since ethylene oxide is a highly toxic gas. Starting with all nozzles closed, nozzles numbered 5, 6, 7, 8 were open to pull vacuum. When sufficient vacuum was pulled in the system, nozzles 5, 6, 7, 8 were closed, and argon was flowing outward of the flask 2 to prevent any substance from coming into the flask. Using a syringe and a needle, n-butyllithium was injected to the flask 2 in order to clean the system, and the argon was shut down. A stir bar was put into the flask 2 in advance and after injecting n-butyllithium into the flask, it started stirring (the flat cylinder under the flask 2 is a stir-plate). After stirring the n-butyllithium for around a minute, the nozzle 6 was crack-opened and slowly to its entirety, so the n-butyllithium has its solvent removed and spread over the flask 2 and 3 to remove any water or oxygen in the system. When n-butyllithium had its solvent removed, liquid nitrogen was placed under the flask 2 to drop its temperature to collect and freeze ethylene oxide from 1. Nozzle 6 was closed, and nozzle 3 was opened to start collecting ethylene oxide with the driving force of pressure difference. Meanwhile, liquid nitrogen was freezing the ampoule 4. After about 10 ml of ethylene oxide was collected in the flask 2, nozzle 3 was closed and nozzle 5 and 6 were opened to pull vacuum on flask 2 to remove any foreign content or residual ethylene oxide. This step is crucial because after this, ethylene oxide was going to be thawed, and if there is any impurity other than ethylene oxide, it could cause an explosion due to its extreme volume expansion. Nozzle 4 was opened for sometime to make sure all the ethylene oxide in between 1 and flask 2 was collected into the flask 2, and

then closed. At this point, nozzle 3, 4, 8 were closed, and 5, 6, 7 were opened. Then nozzle 9 was opened, 5 and 7 were closed, and the liquid nitrogen bath under the flask 2 was changed to cold isopropyl alcohol to slowly bring up the temperature of frozen ethylene oxide. Ampoule 4 was still frozen in the liquid nitrogen bath and started collecting thawed ethylene oxide from the flask 2, again with the driving force of pressure difference. After about 3 mL of ethylene oxide was collected, nozzle 8 was closed. At this point, nozzle 3, 4, 5, 7, 8 were closed, and only 6 was opened. Nozzle 5 and 7 were opened to remove any residual ethylene oxide to vacuum trap. Then ampoule 4 was disassembled from the system and connected to both vacuum line and the previously prepared IS in benzene as shown in the Figure 4.

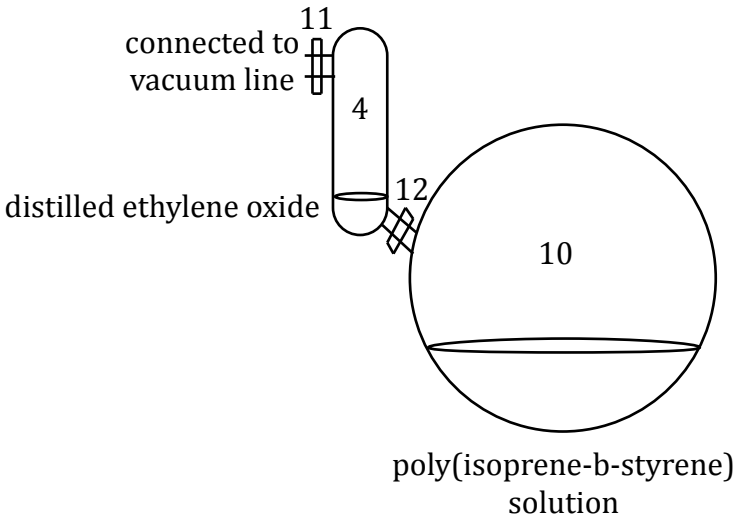

Figure 4. Schematic of experiment set-up to add ethylene oxide block to poly(isoprene-b-styrene) (IS)

Figure 4 shows an ampoule number 4 from the Figure 3 that is connected to the vacuum line, and contains distilled and frozen ethylene oxide. Here, nozzle 11 was opened, and 12 were closed. The nozzle connecting the ampoule 4 to argon tank was opened to fully back-flow twice to make sure that the ampoule 4 has higher pressure than the flask 10, so IS solution would not backflow into the ampoule 4. Then, finally nozzle 12 was opened to let the thawing ethylene oxide will flow into the flask 10 and react with IS solution. The color of the solution turned from bright orange to transparent. After polymerization was complete, the distillation system shown in Figure 4 was all disassembled including the vacuum trap and opened to the hood for longer than 3 hours in order to remove any residual ethylene oxide in the vacuum system.

The ISO solution was stirred overnight. Finally, a mixture of hydrochloric acid (HCl) and methanol was freeze pump-thawed three times, and added to the polymer solution to precipitate the completed poly(isoprene-b-styrene-b-ethylene oxide) (ISO). The solvent was distilled, by freezing and pump-thawing three times, and connected right to the vacuum line for more than 2 hours to remove the solvent, benzene. To extract the final product, a chloroform and water mixture was added to the ISO for phase separation. The solution was vigorously stirred, sat for some time to phase separate, the bottom phase of the chloroform ISO mixture was collected, and the procedure was repeated several times. The very last phase separation was let to stay overnight to get a very fine separation.

To ISO and chloroform mixture, magnesium sulfate powder was added to dry ISO. The solution was stirring, while adding the magnesium sulfate, until it became a uniformly cloudy solution. After the precipitation, this solution was poured into a clean reactor through a filter paper. Then, solvent was removed via distillation and the residue dried on the vacuum line. For further drying, a flask containing phosphorous pentoxide (P_2O_5) was connected between the ISO containing reactor and the vacuum line and kept for 4 days.

The reactor with dried ISO, distilled THF, KCl, and potassium naphthalenide (KN) were brought into the glove box. In the glove box, 117 mg of KCl was added to the distilled THF and stirred. After the KCl was fully dissolved, the solution was added into the dried ISO reactor, and then KN was slowly added while stirring, to reinitiate the poly(isoprene-b-styrene), until the solution became completely green without turning back to its starting color, light yellow. The solution was brought out of the glove box, and the last block, ethylene oxide was distilled, and added to the reinitialized poly(isoprene-b-styrene) solution. After five days of stirring the solution, freeze pump-thawed methanol and HCl was added to terminate the solution, and its color turned from green to yellow. Subsequently, solvent was dried away using the vacuum line. When the vacuum level reached around 1 mbar, the dried polymer was disconnected from the vacuum line, and the mixture of chloroform and water was added for phase separation. Here, because the polymer has ethylene oxide block, it had difficulties separating from water, thus left overnight to finely separate. The next day, its was once more phase-separated, and then filtered through a filter paper. The resulting

polymer-chloroform solution was placed in a rotary evaporator at 40˚C to dry some of the chloroform, but not to completion. The solution was then brought into a syringe with a needle to be slowly dropped into stirring methanol, which is polymer's non-solvent, for the polymer to be precipitated. This continued overnight for its entirety to be precipitated. The next day, methanol was decanted and the precipitation was dried in the rotary evaporator at 40˚C until it was completely dried. Dissolving the final product in THF for GPC showed the PDI showed to be 1.06 for the ISO copolymer, JY06.

3.3 Result and discussion

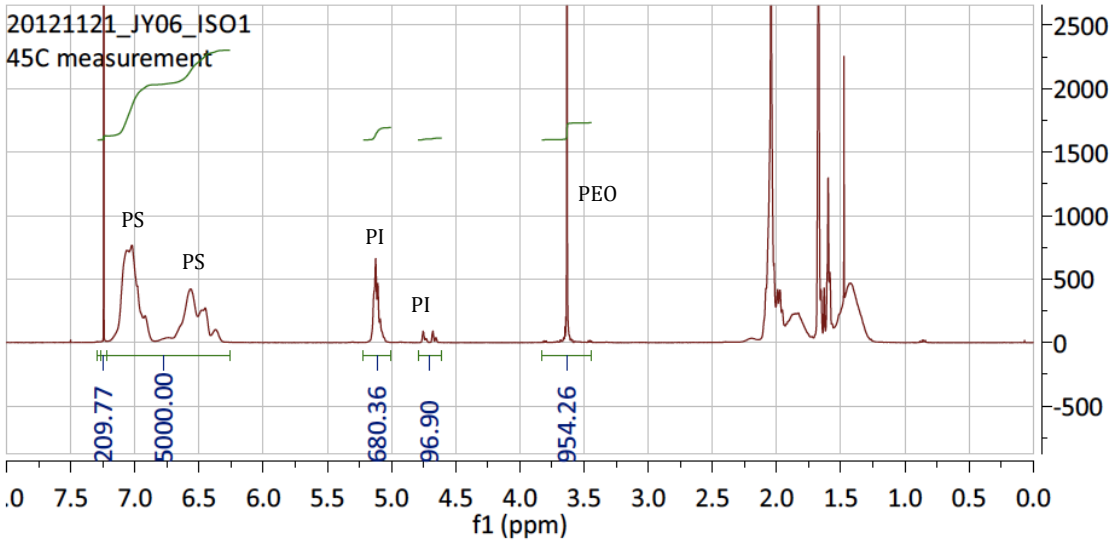

Figure 5. NMR data for PI-PS-PEO

Figure 5 shows the proton nuclear magnetic resonance (NMR) spectrum of polymer, JY06. The numbers below the graph show the integration of the areas under the peaks, suggesting the relative amount of protons for a particular peak. In the NMR shown in Figure 5, the peaks, in sequence, result from protons of chloroform, PS, PS, PI, PI, and PEO, respectively. The final peaks at even lower field are from the 'alkyl region' where all the backbone protons of the macromolecules are included. From the integration results, together, with the molar mass of the PI block, given from GPC, the molar mass of the other blocks of the JY06 can be calculated. In order to do this, the weight percent of each block has to be calculated first, using the sample weight calculated, using the molecular number obtained from the NMR, multiplying it by the molar mass of each block (the molar mass of PI= 68.12 g mol^{-1}, PS=104.16 g mol^{-1}, and PEO=44.05 g mol^{-1}). As mentioned before, the 4^{th} and the 5^{th} peaks represent the PI block. When isoprene is polymerized in benzene, it is polymerized preferably on the 1 and 4 carbon and, in this case, NMR detects carbon 3, giving one hydrogen atom for each block. However, some isoprene is polymerized on carbon 3 and 4, allowing NMR to detect the carbon 1 with two hydrogen atoms for each PI block, and therefore, the 5^{th} peaks include two peaks. This has to be divided by two, to provide the right number of the of PI content. Therefore, the weight of the PI block in NMR sample can be calculated as such.

$$\text{Weight of the PI in NMR sample} = \left(680.36 + \frac{97.90}{2}\right) \times 68.12 = 49,646.54$$

Similarly, the weight of PS in NMR can be calculated as,

$$\text{Weight of the PS in NMR sample} = \left(\frac{5000 - 209.77}{5}\right) \times 104.16 = 99,790.07$$

The 209.77 come from the solvent, chloroform, and are subtracted from the number of moles. Also, because styrene has a benzene ring, and has 5 hydrogen atoms per block, the number of moles is divided by 5, and multiplied by its molar mass, 104.16.

$$\text{Weight of the PEO in NMR sample} = \left(\frac{954.26}{4}\right) \times 44.05 = 10,508.79$$

The PEO block also has 4 hydrogen atoms per block, so the number of moles are divided by 4, and multiplied by the molar mass of PEO, 44.05. The sum of each block gives the weight of JY06 in the NMR sample to be 159,945.40 g mol^{-1}. Now given with the weight of each block in the NMR sample, its weight percent can be calculated as PI, 0.31, PS, 0.624, and PEO, 0.066. The PI molar mass is already

given from GPC as 29021 g mol^{-1} and the molar mass of PS and PEO can be deduced, using the weight percent of each block.

$$\text{Molar mass of PS} = 29021 \times \left(\frac{0.62}{0.31}\right) = 58,416.46$$

$$\text{Molar mass of PEO} = 29021 \times \left(\frac{0.06}{0.31}\right) = 6,178.66$$

To conclude, using NMR and GPC, the molar mass of PI, PS, PEO, and the sum, JY06 were calculated as, 29,021 g mol^{-1}, 58,416.46 g mol^{-1}, 6,178.66 g mol^{-1}, and 93616.13 g mol^{-1}. Due to the large digits, the molar mass of JY06 is often referred as 93K.

The JY06 has a small PEO fraction, which is hydrophilic part, of 6.7 weight percent, compared to the hydrophobic part, PI and PS, which is more than 90 percent of the polymer. This was intentional, in order to study bigger window of inorganic fraction in the system to be able to structure in variety. Its color was white, and had a figure of sphere with a diameter of about 3 ml, weighing about 2 mg per each. This was kept in a sealed glass bottle in a freezer.

Chapter 4.

ISO-aluminosilicate hybrids

4.1 Motivation

Triblock terpolymers to provide more possible structures compared to diblock copolymers. As mentioned in the previous chapter, ISO is suitable for the study of complex triblock copolymer hybrid systems, due to its amphiphilic nature with hydrophobic PI and PS blocks and hydrophilic PEO block. Chatterjee *et al.* presented the experimental phase diagram of ISO system of M_n 's range from 5.8 to 43.0 kg mol^{-1}[20].

Block copolymers have been used as structure-directing agents for functional inorganic materials. Wiesner *et al.* have combined functional materials with block copolymers. Both diblock copolymer and triblock terpolymer derived hybrids have been investigated, in particular with aluminosilicate nanoparticles[21][22][23], which constitute the most deeply studied block copolymer hybrid system to date. Recently, members of the Wiesner group have studied structures of ISO-AlSiO hybrid materials of molar mass of 30~40 kg mol^{-1} as summarized in a morphology map in Figure 6.

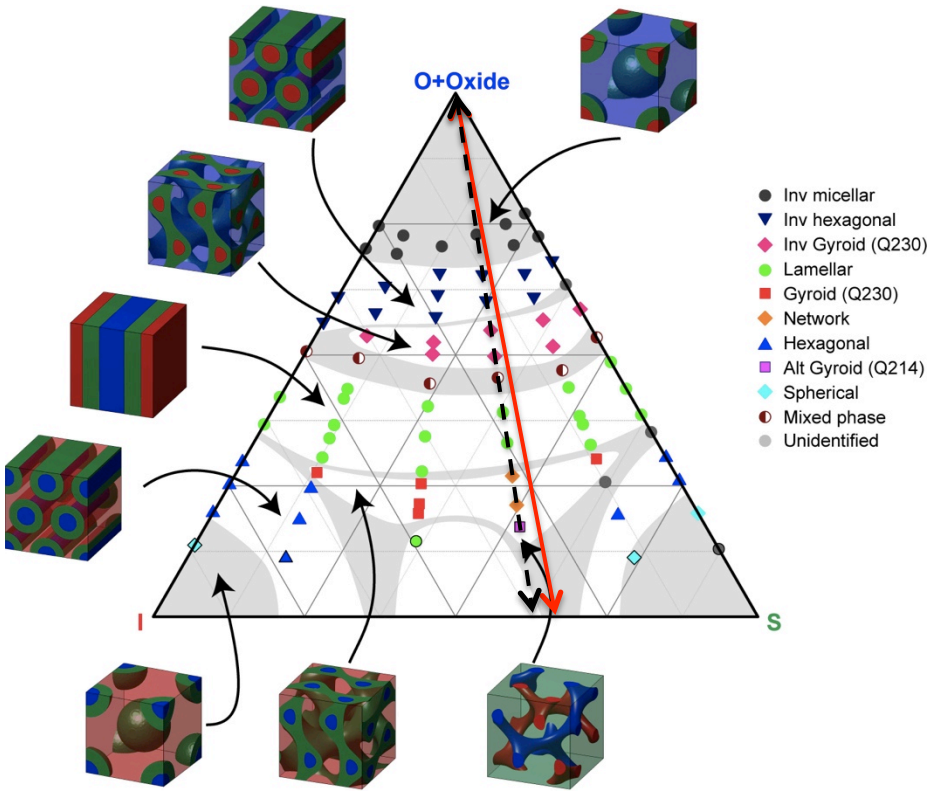

Figure 6. Morphology map of ISO + aluminosilicate NP hybrids

Bates *et al.* have suggested that the triblock terpolymer ISO structure is strongly influenced by the increase of molecular weight and long-range order is lost[24]. The ability to use molecular weight of the parent block copolymer to tailor the length scale of nanostructures would be interesting from the standpoint of achieving designed structures. To this end, the previously described polymer, JY06, was applied to form hybrid materials with aluminosilicate NPs to be compared with results from ISO-1, a triblock terpolymer with similar volume fractions of the blocks, but with lower overall molecular weight. In Figure 6, the dashed black line represents terpolymer ISO-1, and the solid red line represents

terpolymer JY06, with different volume percent of the O block swollen by aluminosilicate.

4.2 Experimental Section

The desired amount of terpolymer JY06 was weighed out and dissolved to be 10 weight-percent in the mixture of dry THF and dry chloroform of 1:1 mass ratio.

During dissolution of JY06 in the solvents, aluminosilicate sol was prepared. The precursor, (3-glycidyloxyproply)trimethoxysilane (GLYMO) (Sigma-Aldrich, CAS No. 2530-83-8) was brought out of the refrigerator to be warmed up to room temperature, then 2.65 g of it was taken out and injected into a vial. Subsequently, 0.73 mL of aluminum tri-sec-butoxide was taken out of the glove box using a syringe and a needle, injected into the vial and stirred until it was uniformly mixed with GLYMO. KCl was added to the solution. After stirring for a couple of minutes, this vial was brought into an ice bath to cool down to 0˚C and stirred for around 10 minutes. 0.135 ml of 0.1 M HCl was prepared and injected dropwise to the vial, while stirring to induce hydrolysis and condensation. At this stage, the solution became cloudy. After the complete injection, the solution was stirred for another 15 minutes. Then, another 0.85 ml of HCl was injected into the solution drop-wise while stirring, one drop every 5 seconds. The solution was stirred for another 20 minutes. At this stage, the solution became clear again. The solid content in the sol solution was 53 wt%. Using this number, the expected weight of fully condensed aluminosilicate was calculated and the desired amount was diluted

to 10 weight-percent in THF. The deserved amount of this solution was injected into the JY06 solution and stirred for 30 minutes before casting. The solution was slowly cast into an aluminum dish that was placed on a glass plate with a dome on top, which in turn sat on top of a hot plate set to 50˚C, and left overnight. After one day of casting, the material had turned into a firm film. A series of 17 films were prepared as shown in Table 2.

Name	Volume fraction			Weight fraction of oxide
JY06	I	S	O+oxide	
JY06-1	0.659	0.286	0.054	0
JY06-2	0.631	0.274	0.095	0.071
JY06-3	0.6596	0.260	0.143	0.151
JY06-4	0.564	0.245	0.191	0.224
JY06-5	0.530	0.231	0.239	0.294
JY06-6	0.493	0.214	0.293	0.366
JY06-7	0.464	0.202	0.335	0.419
JY06-8	0.428	0.186	0.386	0.480

JY06-9	0.392	0.171	0.437	0.538
JY06-10	0.359	0.156	0.485	0.589
JY06-11	0.339	0.148	0.513	0.617
JY06-12	0.316	0.136	0.546	0.650
JY06-13	0.295	0.128	0.576	0.678
JY06-14	0.274	0.119	0.607	0.706
JY06-15	0.253	0.110	0.637	0.733
JY06-16	0.232	0.101	0.667	0.759
JY06-17	0.211	0.092	0.698	0.784
JY06-18	0.189	0.082	0.729	0.810

Table 2. Volume fraction of PI, PS, and PEO in JY06-AlSiO hybrid samples and their weight fraction of oxide

4.3 Result and discussion

The series of JY06 hybrids were analyzed by small-angle x-ray scattering (SAXS) (Cornell High Energy Synchrotron Source (CHESS)), and transmission electron microscopy (TEM) (FEI Tecnai 12 BioTwin TEM). All TEM samples

were sectioned with a cryoultramicrotome (Leica EM UC7/FC7 Cryoultramicrotome) and stained with osmium tetroxide (OsO_4) to render the polyisoprene block dark and to help understand the structures.

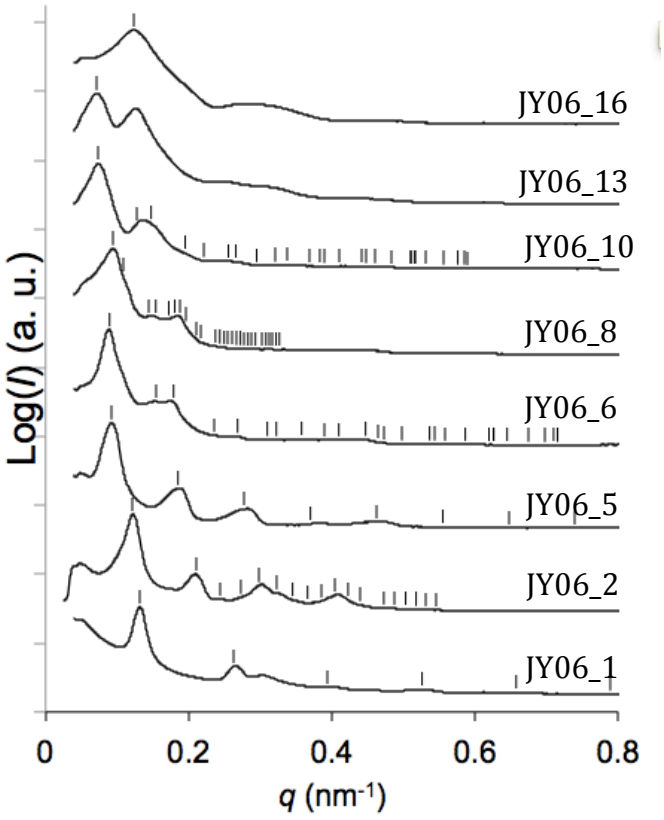

Figure 7. SAXS patterns for selected JY06-AlSiO hybrids.

A SAXS results for the JY06 series is shown in Figure 7. The results for hybrids not shown in Figure 7 were mixed phase or very difficult to interpret. Sample JY06-1 shows a set of peaks consistent with a lamellar structure except an extra peak next to the second reflex. The TEM images for JY06-1 in Figure 8 (a), (b) are consistent with this structure assignment.

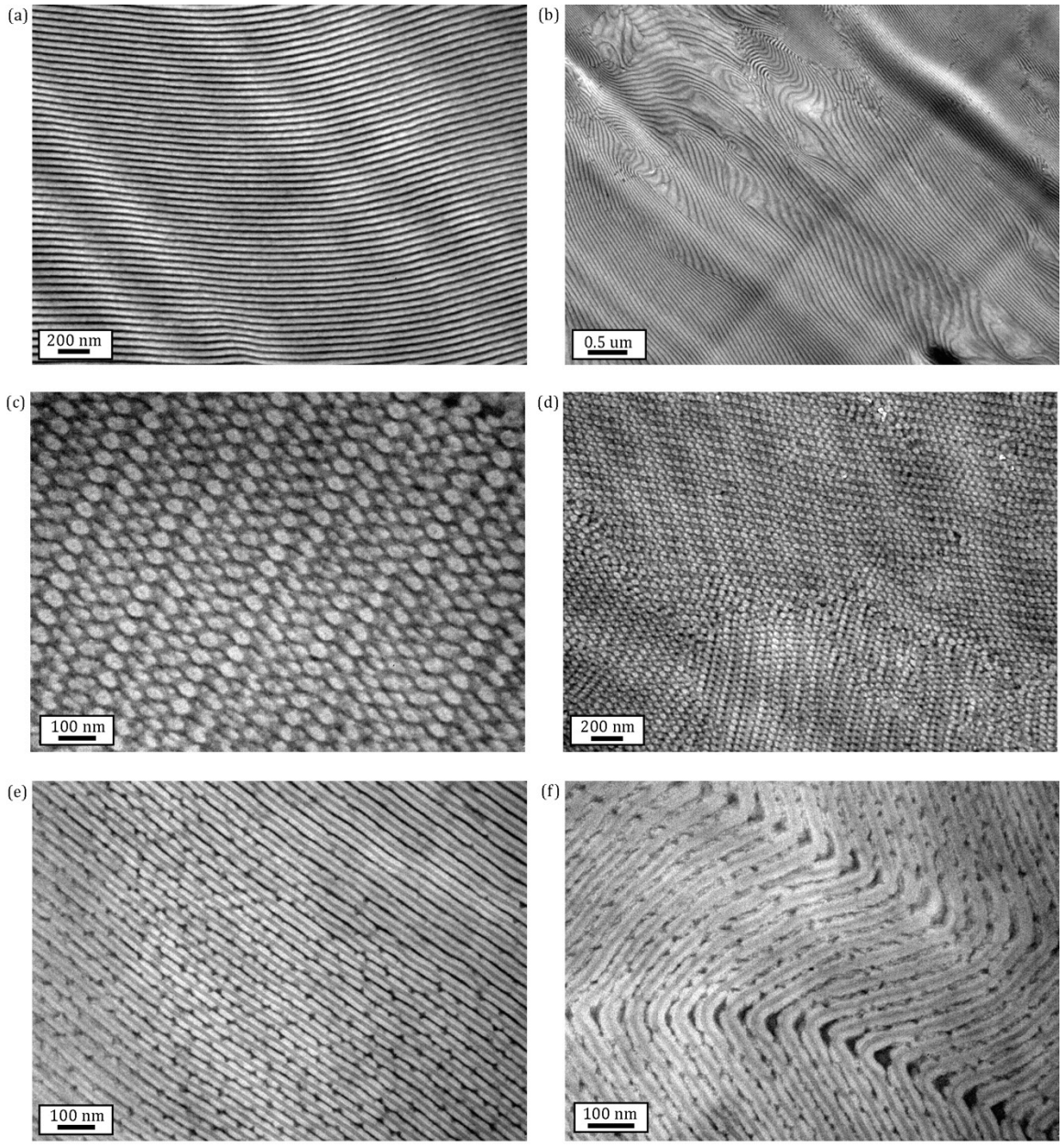

Figure 8. TEM images of JY06-AlSiO hybrid. (a, b) JY06-1 (Lam), (c, d) JY06-2 (Q214), (e, f) JY06-5 (semi-perforated lamellae)

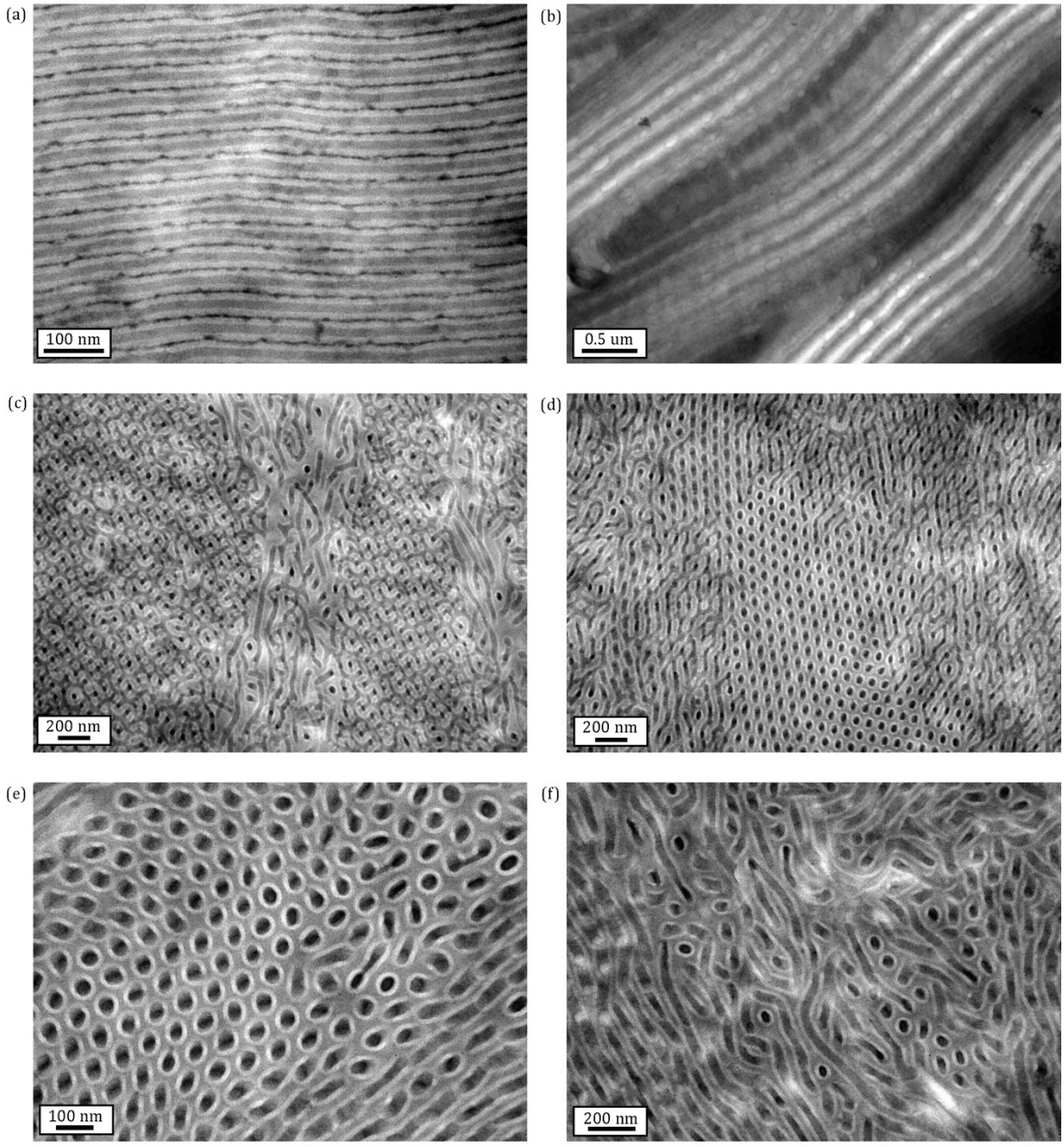

Figure 9. TEM images of JY06-AlSiO hybrids. (a, b) JY06-6 (semi-perforated lamellae), (c, d) JY06-8 (Q230, inv. hex.), (e, f) JY06-10 (inv. hex.)

SAXS and TEM results for sample JY06-2 are consistent with the Q214 structure. The SAXS for sample JY06-5 is consistent with a lamellar structure, which is corroborated by TEM (Figure 8 (e, f)).

JY06-7 will be covered separately later in the chapter.

In TEM sample JY06-8 showed a mixed phase of Q230 and inverse cylinder structure (Figure 9 (c, d)). Furthermore, this sample showed several, around 1 um-diameter-sized (or bigger) particles, which was not seen in other samples (Figure 10). The particles were confirmed by TEM to be composed of aluminosilicate (data not shown).

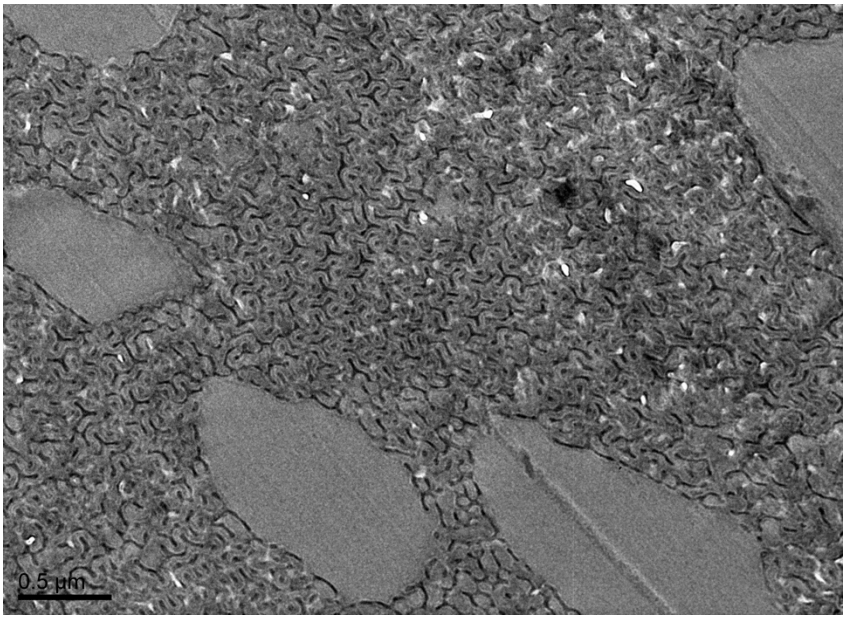

Figure 10. TEM image of unstained JY06-8

These particles were found in repeated experiments with the same aluminosilicate NP loading.

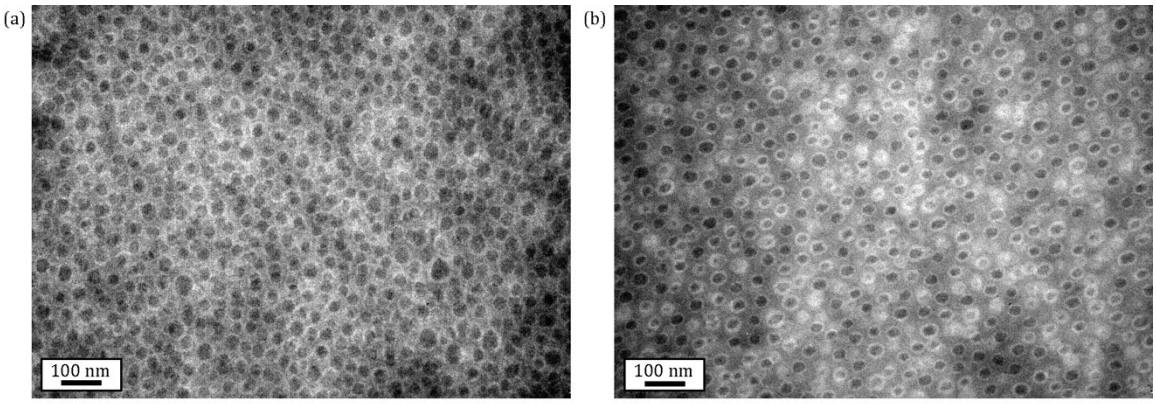

Figure 11. TEM images of JY06-AlSiO hybrids. (a) JY06-13 (inv. micellar), (b) JY06-16 (inv. micellar)

For sample JY06-10 SAXS data could tentatively be indexed with a hexagonal lattice. From TEM, it is shown that it has inverse hexagonal structure (Figure 9 (e, f)). The broadness from SAXS peak may be from the variation of pore size and its position as shown in Figure 11. SAXS patterns of sample JY06-13, and JY06-16 could not be indexed with a lattice (Figure 2). TEM images of these two samples showed micellar morphologies lacking long-range order.

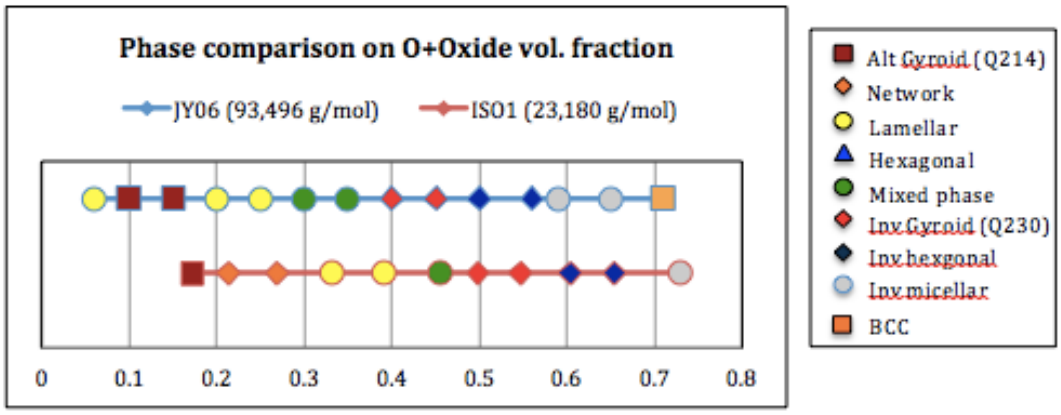

Figure 12. Phase maps for JY06- and ISO-1- hybrid systems.

Figure 12 shows a summary of the results of JY06 based hybrid structures as a function of O + oxide volume fraction and a comparison with results from hybrids of terpolymer ISO-1. The display reveals that JY06 and ISO-1 show a similar sequence of structures overall. However, the sequence for JY06-based hybrids is shifted to lower volume fractions compared to hybrids from ISO-1. This shift may be attributed to the fact that JY06 has a smaller volume fraction of PEO (0.06), as compared to ISO-1 (0.17). For the same O + oxide volume fraction, a lower amount of PEO may lead to a stronger compaction (higher degree of condensation) of the inorganic material, thereby leading to the shift.

Studies have shown that block copolymer systems sometimes show hexagonally perforated lamellar structures, which is a long-lived metastable phase

in a diblock copolymer[12][25]. As mentioned earlier, it was observed that bridges were forming in between lamellar sheets in hybrid JY06-7. In Figure 13 SAXS and TEM images are shown to compare the original lamellae and after the bridges were formed.

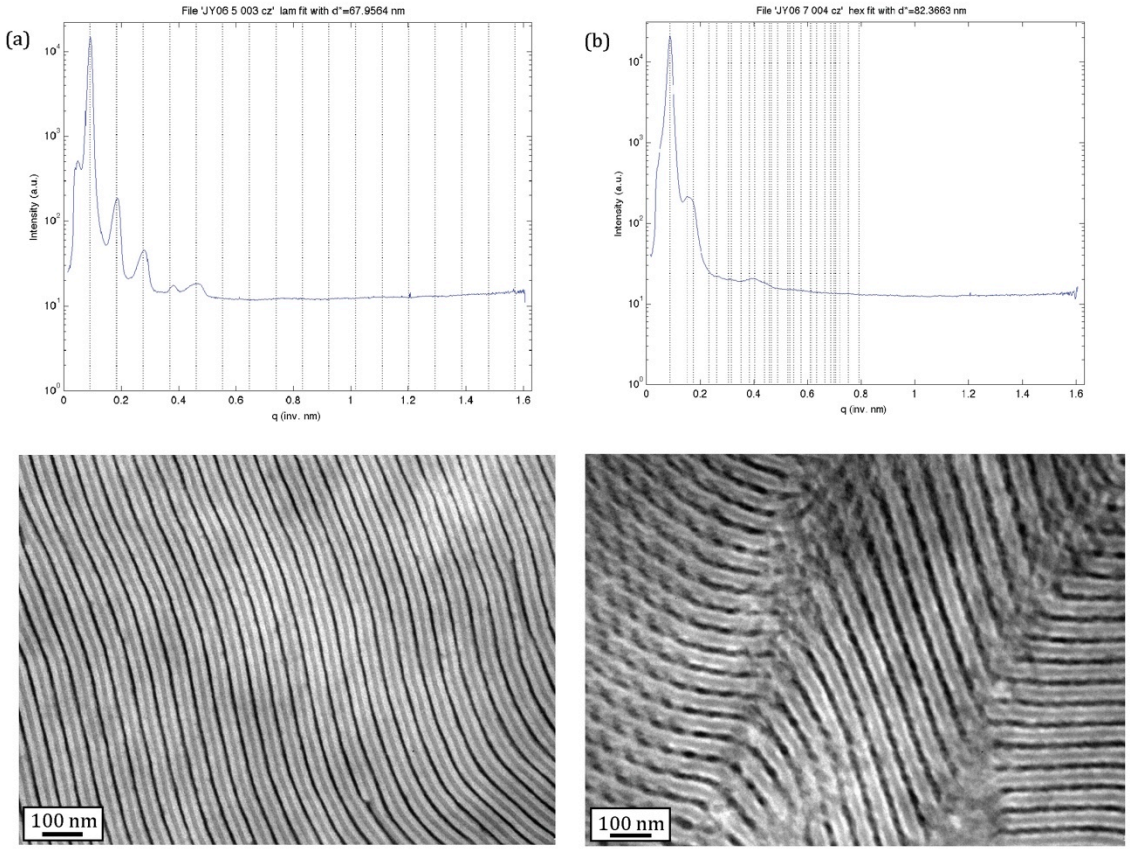

Figure 13. SAXS and TEM data of JY06-5 (Lam), and JY06-7 (hexagonally perforated lamellae)

The TEM in Figure 13 (a) shows lamellae with 3 components of ethylene oxide with aluminosilicate (gray), styrene (white), and isoprene (black). PI domains

appear the darkest due to the staining with OsO_4. The TEM in Figure 13 (b) shows that ethylene oxide with aluminosilicate part is forming bridges in between which originally were lamellae sheets. It is proposed that the bridges consist of ethylene oxide with aluminosilicate surrounded by styrene block, because ethylene oxide with aluminosilicate block cannot have direct contact with isoprene block for its sequence. Possible reasons that the styrene block forming the bridge is hard to see from the image is because, the thickness of the bridge is small, and/or the bridge is perforating into the isoprene block, which is shown black, and the white part could show grey shade by the black around. The unstained TEM image from the same sample is shown in Figure 14 that aluminosilicate part is shown to be the darkest.

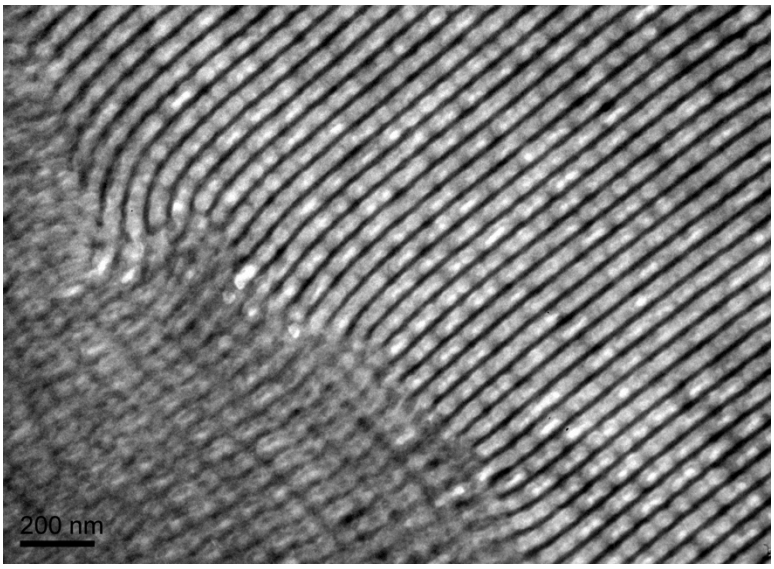

Figure 14. Unstained TEM image of JY06-7 (hexagonally perforated lamellae)

Images with different angles are shown in Figure 15 is shown to clarify the layers in different angles. Figure 15 is stained with OsO_4 and Figure 16 is unstained.

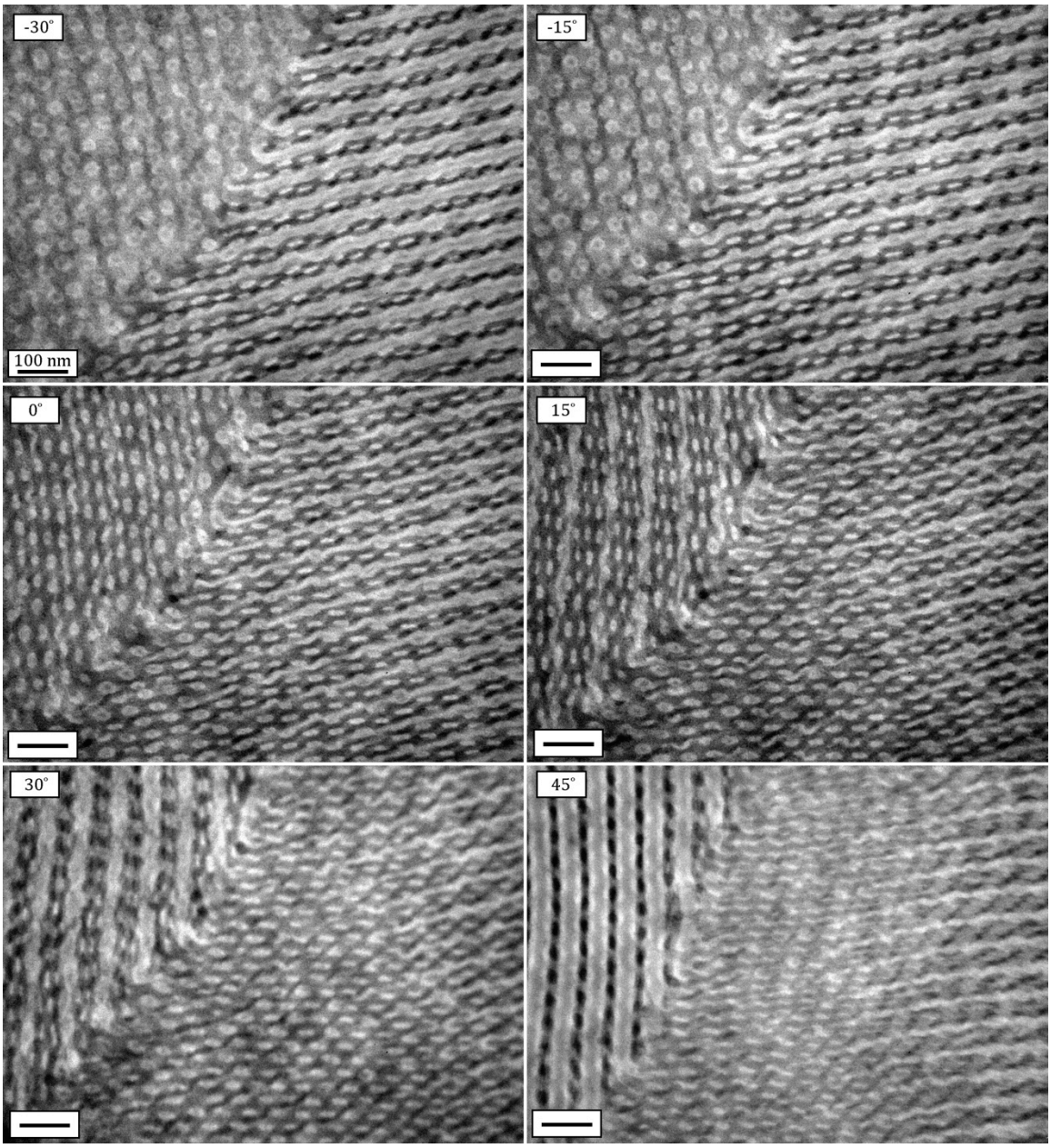

Figure 15. Stained TEM tilt series for JY06-7

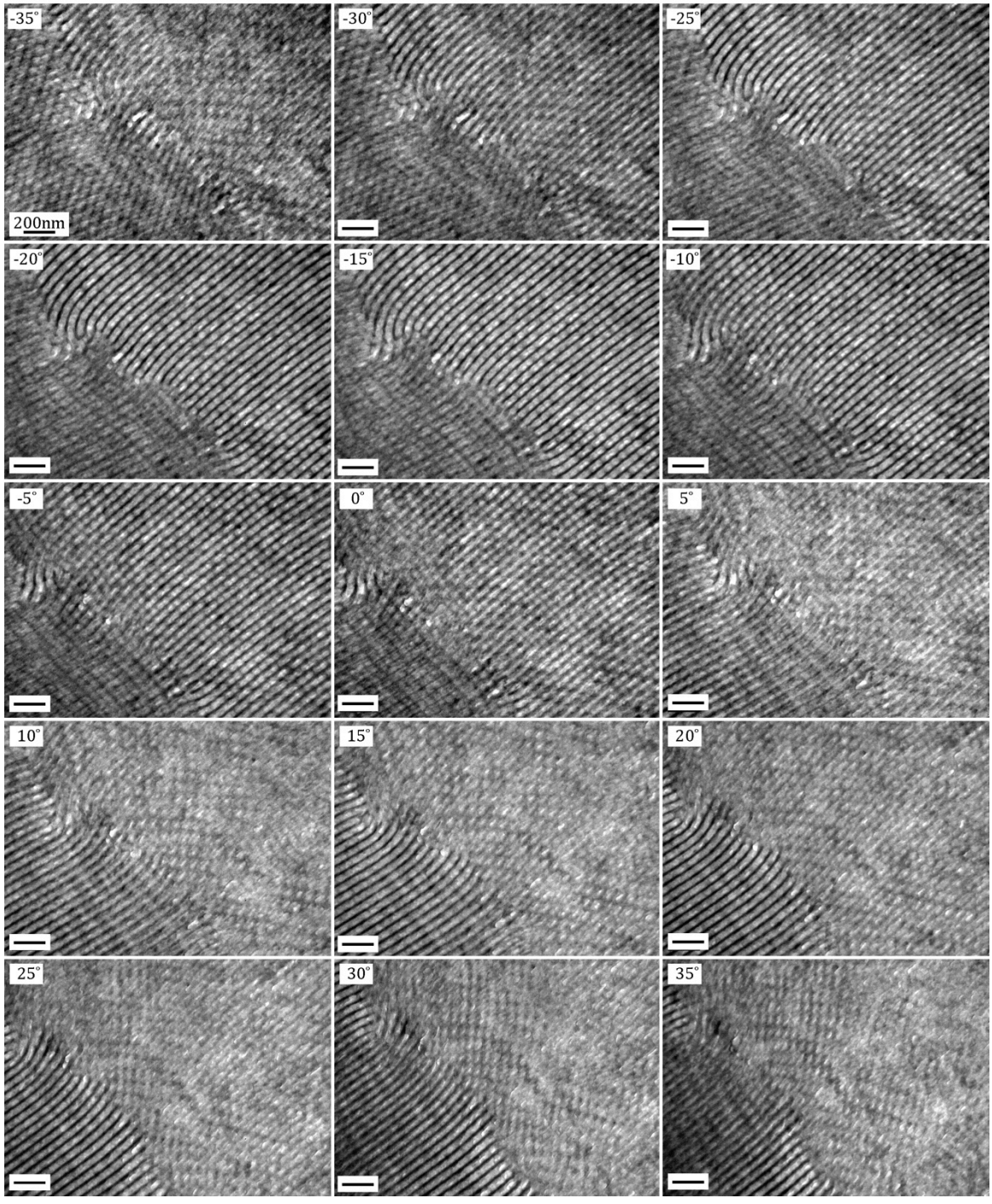

Figure 16. Unstained TEM tilt series for JY06-7

Bates and his coworkers have reported hexagonally perforated layers in IS system [10].

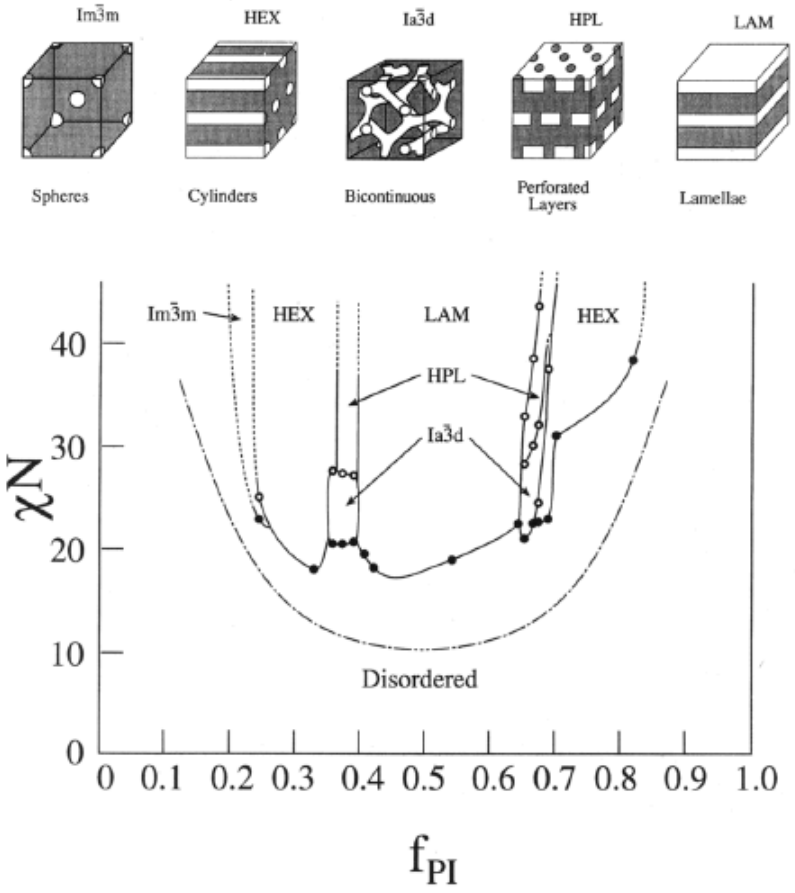

Figure 17. Suggested PI-PS phase diagram by Bates *et al.* [10]

With the study here, and other reported studies, it seems to be reasonable to suggest that JY06-7 shows hexagonally perforated layers as shown in the Figure 18. The structure is represented as a core-shell analogue of the diblock

hexagonally perforated phase, where the polystyrene domain separates the minority PI domain and the majority pillared layer PEO + aluminosilicate domain.

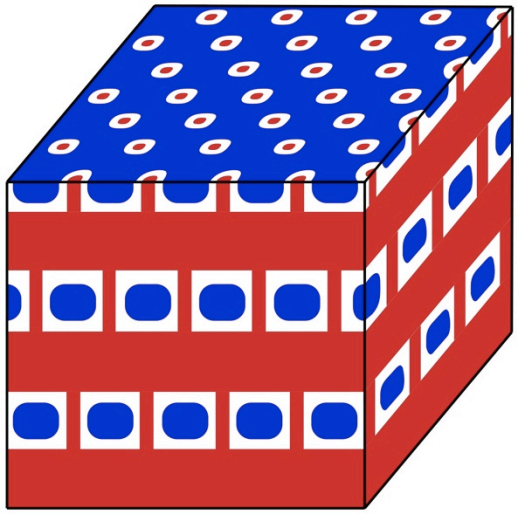

Figure 18. Proposed model for JY06-7 (hexagonally perforated lamellae, red-PEO+oxide, white-PS, blue-PI)

Chapter 5.

ISO-metal oxide hybrids and nitrides

5.1 Motivation

Nanostructured materials have received attention as metal, semiconductor, and ceramic materials for its potential novel properties than its bulk state. Especially mesoporous oxides are highly interesting for their possible use as electrochemical devices and catalysts, which benefit from high surface area, large pore size and fast diffusion. Among other methods template-based[26], sol-gel processes have suggested efficient ways of producing mesoporous oxides with various well-defined structures and pore sizes[27][28]. Using sol-gel chemistry, amphilphilic molecules such as block copolymers and surfactants can be used as structure-direct agents that co-assemble with inorganic precursors into various mesoporous structures. This method is particularly useful for obtaining uniform structural sizes and long-range order in complex three-dimensional network nanostructures. Here, for ISO-based metal oxide hybrids and nitrides from titanium, niobium and gallium have been studied.

Titanium (IV) oxide (TiO_2) has long been studied for its catalytic effects [29][30][31][32]. Because it is a semiconductor, it was studied in the 1980s, for usage in electrochemistry and photovoltaics[33][34]. In the early 1990s, Gratzel and his coworkers found that anatase TiO_2, fabricated through sol-gel chemistry and sintering, could be used in dye-sensitized solar cells (DSCs) [35][36][37]. Studies showed that improvements in connectivity of structure will increase the efficiency [38] [39]. Similarly, niobium (V) oxide (Nb_2O_5) has long been studied

for its possible applications as gas sensors[40], catalysts[41], optical[42] and electrochromic devices[43], batteries[44], and solar cells[45]. The sol-gel route, blending block copolymers and inorganic nanoparticles to co-assemble into various mesoporous structures, has been suggested as a key to control morphology and pore size, by Wiesner[3][46][47], Stucky[5][48], Coakley and MeGehee[49][50], and other researchers. Zukalova and coworkers have discovered that block copolymer templated mesoporous TiO_2 increases the performance remarkably in liquid electrolyte based DSCs[51]. However, there were limitations that their hydrolytic sol-gel process was highly reactive to control the delicate outcome structures, and Pluronic 123, their template polymer from commercial sources, has micropores (~7nm), which became an obstacle for molecular hole-transporter infiltration.

Snaith and coworkers have studied the correlation between the TiO_2 structure and the efficiency of DSCs [52][53][54]. They used poly(isoprene-b-ethylene oxide) for their template and sol-gel chemistry and sintering to build TiO_2 mesoporous structures, and proposed that greater porosity and well-ordered structure will increase the efficiency of DSCs. They also showed that increasing the molecular weight increased the pore size. Triblock terpolymers are known for their ability to control morphology, and the ISO system was reported to have a bigger window to provide Q214 structure, which is a bicontinuous structure with highly connected network pores[14][55]. Recently, it has been reported that titanium nitride (TiN) materials show plasmonic effects and its performance improves in the form of nanostructures [56]–[59]. Finally niobium nitride (NbN)

has attracted great attention in energy and optics field for its potential to show superconductivity [60][61][62].

Here, TiO_2 and Nb_2O_5 was structure-directed by sol-gel chemistry with rather large molar mass 93 kg mol^{-1} ISO and studied to produce long-range, well-ordered structures. Studies also have covered the optimization of nitriding conditions for TiO_2 and Nb_2O_5 mesoporous oxides to maintain their structures with the highest nitrogen to oxygen ratio as TiN and NbN.

Gallium oxide and its nitride were also studied here. Gallium nitride (GaN) is a III-V direct band-gap material with band gap of 3.39eV, is a blue and UV light emitter, having high melting temperature higher than 2500˚C, which suggests possibilities to be used in high-temperature devices. For its benefit of having direct and large band gap, GaN has always been focused on in both research and industry, but for its benefit and challenge, for having high melting temperature, it had not been achieved to produce its own wafer. For this reason, GaN is often grown on substrate, with the least lattice mismatch, and this is often sapphire or zinc oxide. Even for the small mismatch, defects can cause a drop in efficiency, especially when it comes to electronic properties. For the reason, I suggest that sol-gel route will bring a solution to the issue, by synthesizing freestanding mesoporous GaN structures. Here, in the study, through a sol-gel route, gallium oxide has been synthesized first with polymer JY06, and then it was nitrided in an ammonia atmosphere to obtain freestanding GaN structures.

5.2 Experimental Section

5.2.1 Titanium oxide and nitride

93 kg mol^{-1} ISO (JY06) synthesized as introduced in Chapter 3, was dissolved in either a THF/chloroform mixture at 10 wt% or in dry THF at 5 wt%. 37% HCl and 1 ml of dry THF was added to a different vial, then, 2.5 mL titanium (IV) isopropoxide was added to the solution and stirred for 5 minutes. Subsequently, 4 ml of dry THF was added to the vial and stirred for another 2 minutes.

For one set of experiments, 7 hybrid samples were made, each with 50 mg of JY06 dissolved in dry THF to be 5 wt% JY06 solutions. Each were named; JY06-TiO_2-A, JY06-TiO_2-B, JY06-TiO_2-C, JY06-TiO_2-D, JY06-TiO_2-E, JY06-TiO_2-F, and JY06-TiO_2-G. For these samples, 0.1, 0.2, 0.26, 0.28, 0.3, 0.35, 0.45 ml of sol solution was added to the 5 wt% JY06 solution, respectively. The solution was stirred overnight. After about 24 hours, the solution was casted on Teflon dishes, placed on a glass plate with a glass dome on top, on a hot plate at 35~50 ˚C. The films were left overnight to make sure they are fully dried. TEM sample were sectioned through cryoultramictrotoming. Samples were calcined in an air furnace with 1˚C/minute ramping up to 450˚C and kept at 450˚C for 3 hours to completely burn off the polymer, leaving TiO_2 free-standing structure, which was later analyzed with scanning electron microscopy (SEM) (Tescan Mira3 FESEM). Some of the calcined samples were nitrided in ammonia atmosphere at either 600˚C or 850˚C with different ramping rate and analyzed with SEM.

5.2.2 Niobium oxide and nitride

93 kg mol^{-1} ISO (JY06) synthesized as introduced in Chapter 3, was prepared in dry THF to be 5 wt% and stirred until it is completely dissolved. Meanwhile, sol solution was prepared as follow: 0.375 mL of fuming 37 wt% HCl was injected into a 4 mL Teflon-lined cap vial with a stir bar using microliter pipette for accuracy. While this was stirring, 2.5 mL of dry THF and 0.64 mL of niobium (V) ethoxide were brought out of the glove box. 1 mL of the dry THF was injected to the HCl stirring vial, then the niobium (V) ethoxide was injected into the solution. White fume was produced in the procedure. The solution was stirred vigorously for 5 minutes, then the rest of the THF was injected and stirred for another 2 minutes. A syringe with a needle drew up the complete sol solution to inject into the 1 mL of 5 wt% JY06 solution each, prepared as explained earlier. In total 6 samples were made, each named as JY06-Nb_2O_5-A, JY06-Nb_2O_5-B, JY06-Nb_2O_5-C, JY06-Nb_2O_5-D, JY06-Nb_2O_5-E, JY06-Nb_2O_5-F, JY06-Nb_2O_5-G, with the aliquot sol amount of 0.1, 0.2, 0.26, 0.28, 0.3, 0.35, 0.45, respectively. The solutions were stirred for about 24 hours. This was then poured into a Teflon dish and placed in between a glass dish on the bottom and a glass dome on top to slow down the casting process performed at 35˚C. This seemed to dry in about three hours, but it was kept overnight for its completion. The samples then were brought into a vacuum oven for annealing at 130˚C for 3 hours, for further crosslinking. TEM samples were prepared by cryomicrotoming to be 70nm thick. Freestanding

oxide samples were prepared by calcining the hybrid in air furnace with 1˚C/minute ramping up to 450˚C and kept at 450˚C for 3 hours to completely burn off the polymer. Samples were later analyzed with SEM. Some of the calcined samples were nitrided in ammonia atmosphere at either 600˚C or 850˚C with different ramping rate and analyzed with SEM.

5.2.3 Gallium oxide and nitride

1 mL of JY06 solution in dry THF was prepared to be 5 wt% per sample. A precursor for gallium oxide, gallium ethoxide, a syringe with a needle, and dry butanol and dry THF were taken out of the glove box, then the butanol was injected into gallium ethoxide showing white fume when mixing, and then THF was injected into the solution. The solution remained clear through out the processes. This was stirred overnight, and casted at 35˚C overnight, covered in between a glass slide on the bottom and a glass dome on top. The samples had white color. The samples were then nitrided in ammonia atmosphere with ramping rate of 1˚C/min and remained at 800˚C for 6 hours, and then cooled down to room temperature.

5.3 Results and discussion

5.3.1 Titanium oxide and nitride

Here, the goal of the study was to achieve long-range order with the most porosity. First, a series of JY06-TiO_2 hybrid samples with weight percent TiO_2 of 14, 25, 30, 36, 42, as given from TGA, were made as introduced in the experimental section. First, casting condition method similar to what was used for ISO-aluminosilicate hybrid was used. JY06 was dissolved in the mixture of THF and chloroform to be 10wt% solution and made into TiO_2 hybrid as explained in the experimental section. This was then poured on a Teflon dish and placed on top of a glass dish covered with a glass dome. This was brought to a hot plate and kept at 50˚C. The solution seemed to dry in about an hour, but to make sure it was completed, it was kept overnight, and further annealed in a vacuum oven at 130˚C for 3 hours. The hybrid samples were characterized with SEM and SAXS. SEM images showed some ordered structures, such as gyroid and hexagonal structures, but SAXS showed that they did not have long-range order.

It had been reported that slowing the casting condition would help introducing long-range order[63]. Also, it was empirically fount that chloroform does not help obtaining well-ordered structures for the ISO-TiO_2 hybrid system. Therefore, for the second series (JY06-TiO_2-2 series), three changes were made in the casting conditions. First, to induce slower casting, 35˚C instead of 50˚C was used as casting temperature. Second, an extra reservoir of THF was placed in the dome. Third, THF instead of THF/chloroform mixture was used as the solvent to dissolve JY06.

The SAXS date for the second series prepared using this new casting protocol is shown in the Figure 19.

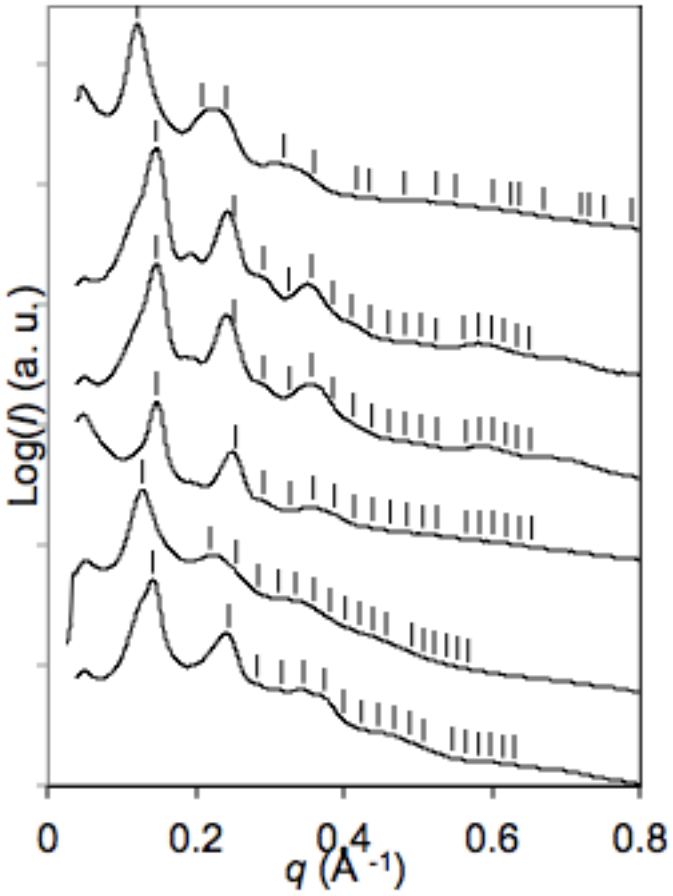

Figure 19. SAXS data for JY06-TiO_2 hybrid series. Sample name (fitting, inorganic weight percent) from the bottom: JY06-TiO_2-2A (Q214, 18.16), JY06-TiO2-2B (Q214, 21.17), JY06- TiO_2-2C (Q214, 25.31), JY06- TiO_2-2D (Q214, 24.25), JY06-TiO_2-2E (Q214, 25.98), and JY06-TiO_2-2F (HEX, 28.57)

From the bottom to top, the sample names are JY06-TiO_2-2A, JY06-TiO_2-2B, JY06-TiO_2-2C, JY06-TiO_2-2D, JY06-TiO_2-2E, JY06-TiO_2-2F, with TiO_2 weight percent of 18.2, 21.2, 25.3, 24.2, 26, and 28.6, respectively. The peaks were all fitted to Q214 except the top one, JY06-TiO_2-2F, which was fitted to a hexagonal lattice. From SAXS patterns, all samples showed exquisite long-range-order. JY06-TiO_2-2A was selected to be nitrided under ammonia atmosphere at 600˚C for 6 hours with the ramping rate of 350˚C per hour. The Q214 structure was retained after nitridation, as seen in Figure 20.

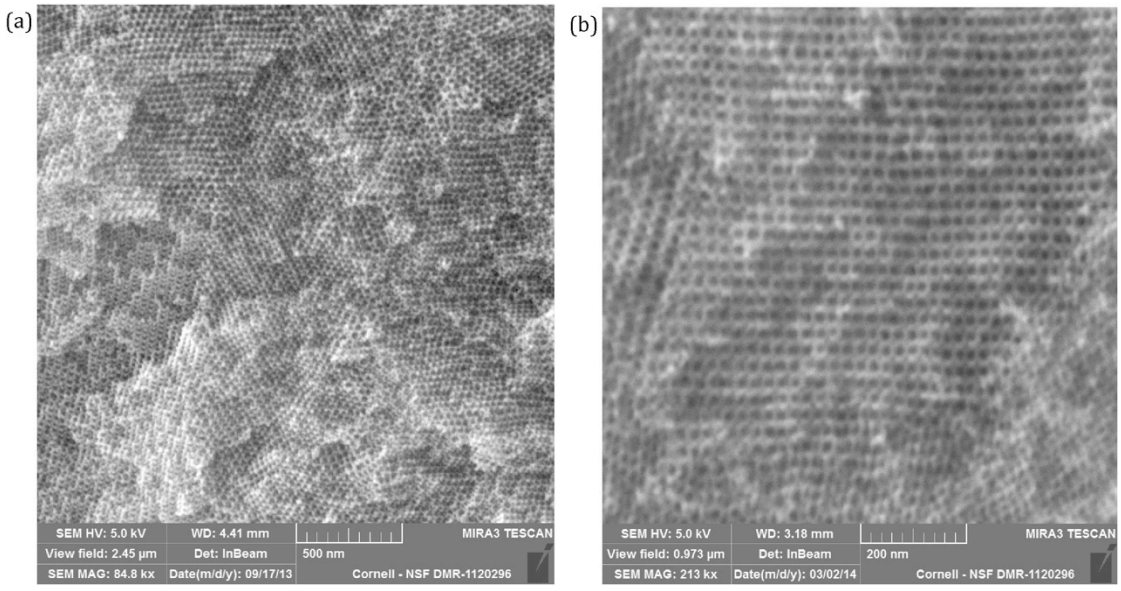

Figure 20. (a) TiO_2 (b) TiN

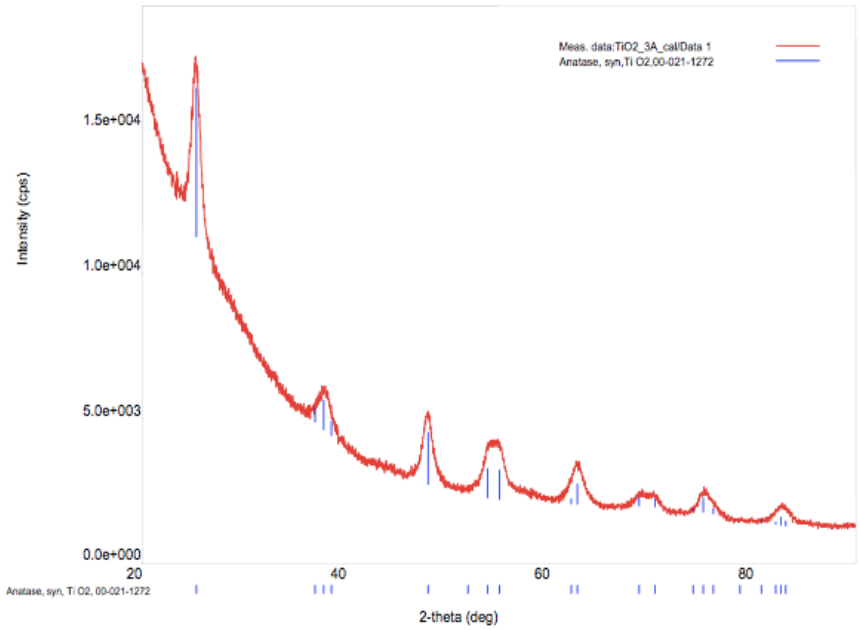

Figure 21. XRD of calcined ISO-TiO_2 hybrid

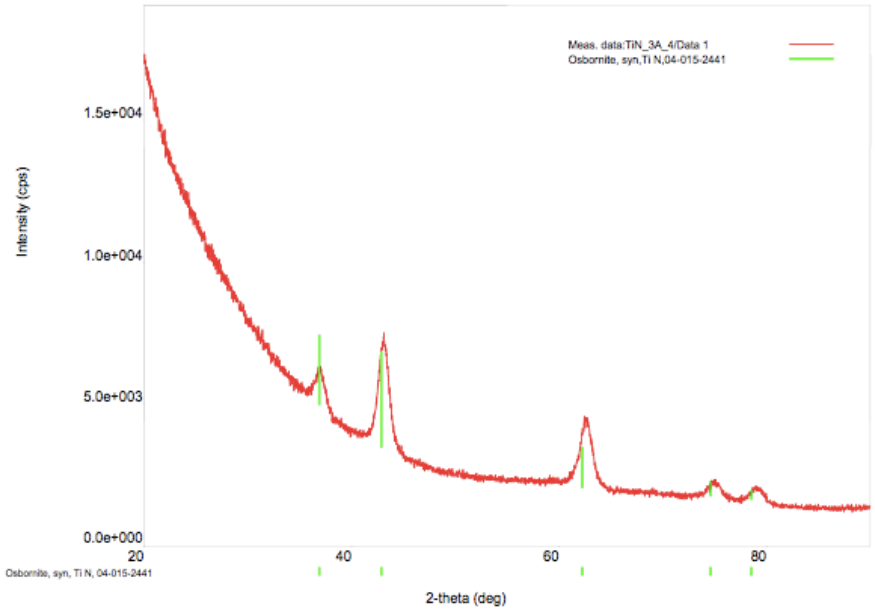

Figure 22. XRD of nitrided TiO_2

XRD was taken for both calcined ISO-TiO_2 hybrid (Fig. 21), and nitrided TiO_2 (Fig. 22). It is shown that the crystalline oxygen peaks from Figure 21, are not found in Figure 22, meaning that the material was successfully transformed into TiN retaining its network Q214 structure even after the harsh temperature treatment and atom exchange of oxygen into nitrogen. From Scherrer's equation, the domain sizes for TiO_2 and TiN were, 7.6 nm and 7.0 nm, respectively.

5.3.2 Niobium oxide and nitride

The goal for the experiments was to achieve well-ordered structures of JY06-Nb_2O_5 hybrid films and optimize the system to retain the structure after calcination and nitridation.

Similar to TiO_2 system, the slow casting protocol was also applied to the Nb_2O_5 system: 35˚C casting temperature and having extra reservoir of THF in the casting system, which was covered with a glass dome. This resulted in unexpectedly well-ordered structures, which is uncommon for high molecular weight polymer because its chain is too long that it makes it harder to arrange them in structure with a long-range order.

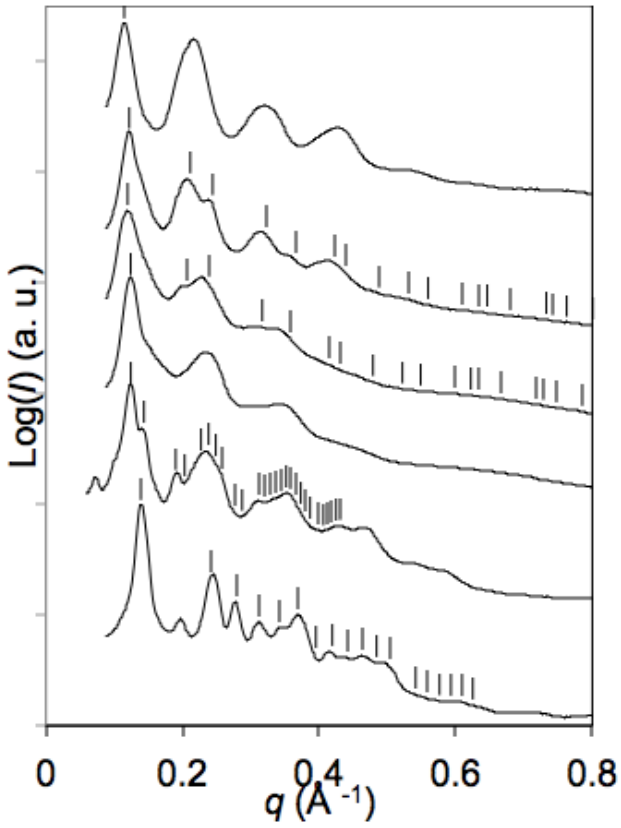

Figure 23. SAXS data for JY06-Nb_2O_5 hybrid series. Sample name (fitting, inorganic weight percet) from the bottom: JY06-Nb_2O_5-A (Q214, 12.1), JY06-Nb_2O_5-B (Q230, 26.1), JY06-Nb_2O_5-C (1^{st} peak, 31.3), JY06-Nb_2O_5-D (HEX, 33.3), JY06-Nb_2O_5-E (HEX, 34.4), and JY06-Nb_2O_5-F (1^{st} peak, 37)

Alternating gyroid (Q214), double gyroid (Q230), and hexagonal structures were obtained from the set, as shown by SAXS analysis (Fig. 23). From the bottom to top, it shows how the structure progresses along with the increase of inorganic material in the system. Especially it is noted that JY06-Nb_2O_5-A and JY06-Nb_2O_5-B show impressively clear SAXS peaks, suggesting the existence of well-ordered,

long-range structures. Also from the SAXS data, JY06-Nb_2O_5-B has 123.7 nm d-spacing, which makes it even more surprising that the peaks are clear and well-fitted to a Q230 lattice. The hybrid film was then analyzed after calcination and nitridation, as described in the experimental section, which succeeded retaining the Q214, even after the harsh temperature treatment.

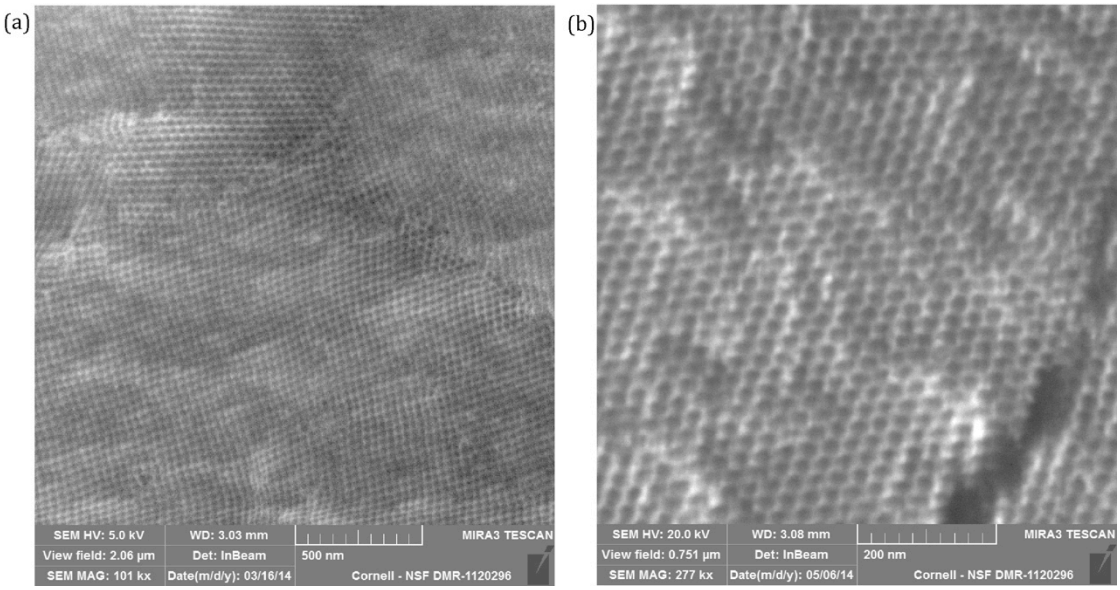

Figure 24. SEM images of (a) Nb_2O_5, and (b) NbN, both maintaining alternating gyroid (Q214) structure.

5.3.3 Gallium oxide and nitride

The goal for this experiment was to find a sol-gel route combining the JY06 and gallium precursor to fabricate free-standing mesoporous gallium oxide, and

eventually its nitride structure. After many trials with different solvents and conditions, butanol was found to stabilize the system, and with the right amount of the gallium precursor, gallium ethoxide, and THF the material would successfully self-assemble into a mesoporous JY06-Ga_xO_y hybrid structure as shown in the TEM image in Figure 25.

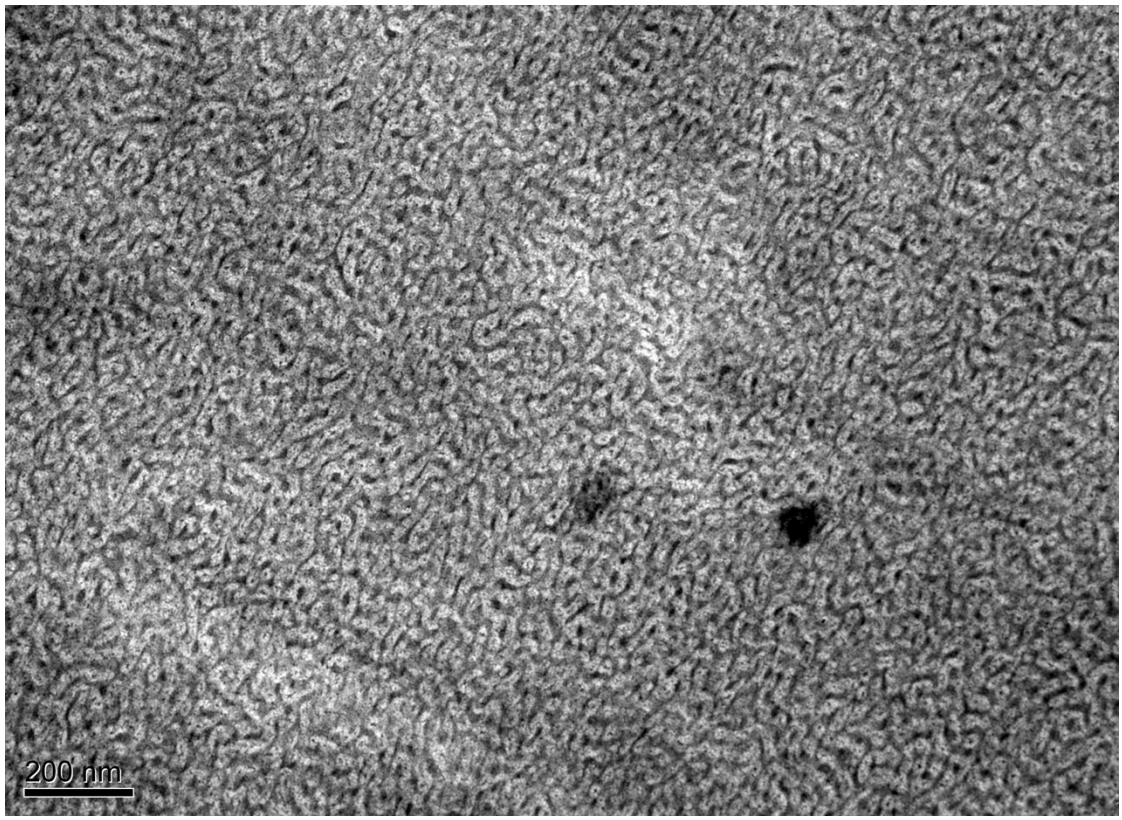

Figure 25. TEM image of JY06-$Ga(EtO)_3$-BuOH

This was then directly nitrided in ammonia atmosphere, which is shown in the SEM images in Figure 26. The images prove that after the nitridation, the material

formed free-standing mesoporous structures. The film color was yellow after nitridation as shown in Figure 27 suggesting that GaN was formed.

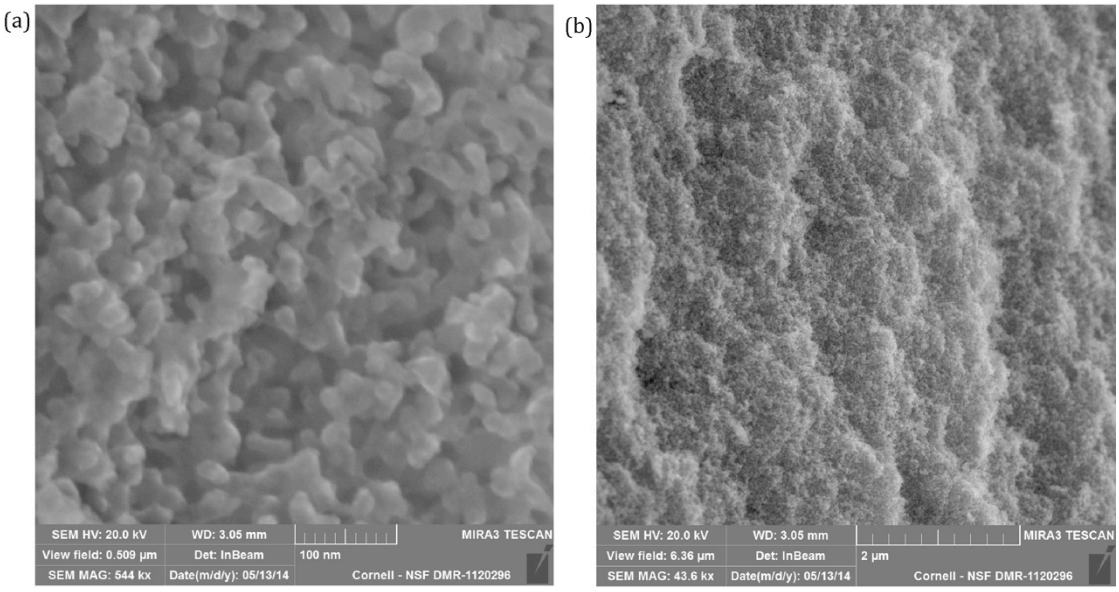

Figure 26. SEM images of JY06-Ga(EtO)$_3$-BuOH in (a) 544 kx (b) 43.6 kx

Figure 27. Image of GaN after the nitradiition

Reference

[1] E. W. Cochran, C. J. Garcia-Cervera, and G. H. Fredrickson, "Stability of the Gyroid Phase in Diblock Copolymers at Strong Segregation," *Macromolecules*, vol. 39, no. 7, pp. 2449–2451, Apr. 2006.

[2] S. C. Warren, L. C. Messina, L. S. Slaughter, M. Kamperman, Q. Zhou, S. M. Gruner, F. J. DiSalvo, and U. Wiesner, "Ordered mesoporous materials from metal nanoparticle-block copolymer self-assembly.," *Science*, vol. 320, no. 5884, pp. 1748–52, Jun. 2008.

[3] M. Templin, "Organically Modified Aluminosilicate Mesostructures from Block Copolymer Phases," *Science (80-.).*, vol. 278, no. 5344, pp. 1795–1798, Dec. 1997.

[4] M. Kamperman, C. B. W. Garcia, P. Du, H. Ow, and U. Wiesner, "Ordered mesoporous ceramics stable up to 1500 degrees C from diblock copolymer mesophases.," *J. Am. Chem. Soc.*, vol. 126, no. 45, pp. 14708–9, Nov. 2004.

[5] P. Yang and D. I. Margolese, "Generalized syntheses of large-pore mesoporous metal oxides with semicrystalline frameworks," vol. 396, no. November, pp. 6–9, 1998.

[6] Y. Yamauchi, A. Sugiyama, R. Morimoto, A. Takai, and K. Kuroda, "Mesoporous platinum with giant mesocages templated from lyotropic liquid crystals consisting of diblock copolymers.," *Angew. Chem. Int. Ed. Engl.*, vol. 47, no. 29, pp. 5371–3, Jan. 2008.

[7] M. W. Matsen and F. S. Bates, "Unifying Weak- and Strong-Segregation Block Copolymer Theories," *Macromolecules*, vol. 29, no. 4, pp. 1091–1098, Jan. 1996.

[8] L. Leiblert, "Theory of Microphase Separation in Block Copolymers," vol. 1617, no. 10, pp. 1602–1617, 1980.

[9] G. Floudas, B. Vazaiou, F. Schipper, R. Ulrich, U. Wiesner, H. Iatrou, and N. Hadjichristidis, "Poly (ethylene oxide- b -isoprene) Diblock Copolymer Phase Diagram," pp. 2947–2957, 2001.

[10] A. K. Khandpurj, S. Farster, F. S. Bates, I. W. Hamley, and A. J. Ryan, "Diblock Copolymer Phase Diagram near the Order-Disorder Transition," pp. 8796–8806, 1995.

[11] Y. Matsushita, J. Suzuki, and M. Seki, "Surfaces of tricontinuous structure formed by an ABC triblock copolymer in bulk," *Phys. B Condens. Matter*, vol. 248, no. 1–4, pp. 238–242, Jun. 1998.

[12] S. Brinkmann, R. Stadler, and E. L. Thomas, "New Structural Motif in Hexagonally Ordered Cylindrical Ternary (ABC) Block Copolymer Microdomains," *Macromolecules*, vol. 31, no. 19, pp. 6566–6572, Aug. 1998.

[13] U. Breiner, U. Krappe, E. L. Thomas, and R. Stadler, "Structural Characterization of the 'Knitting Pattern' in Polystyrene-block-poly(ethylene-co-butylene)-block-poly(methyl methacrylate) Triblock Copolymers," *Macromolecules*, vol. 31, no. 1, pp. 135–141, Jan. 1998.

[14] T. S. Bailey, C. M. Hardy, T. H. Epps, and F. S. Bates, "A Noncubic Triply Periodic Network Morphology in Poly (isoprene- b -styrene- b -ethylene oxide) Triblock Copolymers," pp. 7007–7017, 2002.

[15] U. Breiner, U. Krappe, V. Abetz, and R. Stadler, "Cylindrical morphologies in asymmetric ABC triblock copolymers," *Macromol. Chem. Phys.*, vol. 198, no. 4, pp. 1051–1083, 1997.

[16] U. Krappe, R. Stadler, and I. Voigt-Martin, "Chiral Assembly in Amorphous ABC Triblock Copolymers. Formation of a Helical Morphology in Polystyrene-block-polybutadiene-block-poly(methyl methacrylate) Block Copolymers," *Macromolecules*, vol. 28, no. 13, pp. 4558–4561, Jun. 1995.

[17] R. Stadler, T. C. Auschra, J. Beckmann, and I. Voigt-martin, "Morphology and Thermodynamics of Symmetric Poly (A-block-B-block-C) Triblock Copolymers," pp. 3080–3091, 1995.

[18] Y. Mogi, M. Nomura, H. Kotsuji, K. Ohnishi, Y. Matsushita, and I. Noda, "Superlattice Structures in Morphologies of the ABC Triblock Copolymers," *Macromolecules*, vol. 27, no. 23, pp. 6755–6760, Nov. 1994.

[19] G. M. Whitesides and M. Boncheva, "Beyond molecules: self-assembly of mesoscopic and macroscopic components.," *Proc. Natl. Acad. Sci. U. S. A.*, vol. 99, no. 8, pp. 4769–74, Apr. 2002.

[20] J. Chatterjee, S. Jain, and F. S. Bates, “Comprehensive Phase Behavior of Poly (isoprene- b -styrene- b -ethylene oxide) Triblock Copolymers,” pp. 2882–2896, 2007.

[21] M. C. Orilall, F. Matsumoto, Q. Zhou, H. Sai, F. J. Disalvo, and U. Wiesner, “One-Pot Synthesis of Platinum-Based Nanoparticles Incorporated into Mesoporous Niobium Oxide - Carbon Composites for Fuel Cell Electrodes,” no. 19, pp. 9389–9395, 2009.

[22] B. C. Garcia, M. Kamperman, R. Ulrich, A. Jain, S. M. Gruner, and U. Wiesner, “Morphology Diagram of a Diblock Copolymer−Aluminosilicate Nanoparticle System,” *Chem. Mater.*, vol. 21, no. 22, pp. 5397–5405, Nov. 2009.

[23] M. Stefik, S. Mahajan, H. Sai, T. H. Epps, F. S. Bates, S. M. Gruner, O. F. J. Disalvo, and U. Wiesner, “Ordered Three- and Five-ply Nanocomposites from ABC Block Terpolymer Microphase Separation with Niobia and Aluminosilicate Sols,” vol. 20, no. 5, pp. 5466–5473, 2009.

[24] T. H. Epps and F. S. Bates, “Effect of Molecular Weight on Network Formation in Linear ABC Triblock Copolymers,” vol. 230, pp. 2676–2682, 2006.

[25] G. E. S. Toombes, S. Mahajan, M. Thomas, P. Du, M. W. Tate, S. M. Gruner, and U. Wiesner, “Hexagonally Patterned Lamellar Morphology in ABC Triblock Copolymer/Aluminosilicate Nanocomposites,” *Chem. Mater.*, vol. 20, no. 10, pp. 3278–3287, May 2008.

[26] a Mozalev, M. Sakairi, I. Saeki, and H. Takahashi, “Nucleation and growth of the nanostructured anodic oxides on tantalum and niobium under the porous alumina film,” *Electrochim. Acta*, vol. 48, no. 20–22, pp. 3155–3170, Sep. 2003.

[27] J. Y. U, X. Zhao, and Q. Zhao, “Effect of surface structure on photocatalytic activity of TiO 2 thin films prepared by sol-gel method,” pp. 7–14, 2000.

[28] B. Ohtani, K. Iwai, S. Nishimoto, and T. Inui, “Electrochromism of Niobium Oxide Thin Films Prepared by the Sol-Gel Process,” no. 9, pp. 7–10, 1994.

[29] M. Anpo, “Photocatalysis on titanium oxide catalysts,” vol. 1, pp. 169–179, 1997.

[30] S. Matsuda, “Applied Catalysis, 8 (1983) 149-165,” vol. 8, pp. 149–165, 1983.

[31] D. Chen, D. Yang, Q. Wang, and Z. Jiang, “Effects of Boron Doping on Photocatalytic Activity and Microstructure of Titanium Dioxide Nanoparticles,” *Ind. Eng. Chem. Res.*, vol. 45, no. 12, pp. 4110–4116, Jun. 2006.

[32] P. Panagiotopoulou, a. Christodoulakis, D. I. Kondarides, and S. Boghosian, “Particle size effects on the reducibility of titanium dioxide and its relation to the water–gas shift activity of Pt/TiO2 catalysts,” *J. Catal.*, vol. 240, no. 2, pp. 114–125, Jun. 2006.

[33] C. J. Barbe, F. Arendse, P. Comte, M. Jirousek, F. Lenzmann, V. Shklover, and M. Gra, “Nanocrystalline Titanium Oxide Electrodes for Photovoltaic Applications,” vol. 71, pp. 3157–3171, 1997.

[34] T. A. Heimer, C. A. Bignozzi, and G. J. Meyer, “Molecular Level Photovoltaics: The Electrooptical Properties of Metal Cyanide Complexes Anchored to Titanium Dioxide,” pp. 11987–11994, 1993.

[35] O. Brian, M. Grstzel, and D. Fitzmaurice, “Optical electrochemistry I : steady-state spectroscopy of conduction-band electrons in a metal oxide semiconductor electrode,” vol. 183, no. I, pp. 89–93, 1991.

[36] Y. Tachibana, J. E. Moser, M. Gra, D. R. Klug, J. R. Durrant, and Ä. P. Fe, “Subpicosecond Interfacial Charge Separation in Dye-Sensitized Nanocrystalline Titanium Dioxide Films,” vol. 3654, no. 96, pp. 20056–20062, 1996.

[37] U. Bach, P. Comte, J. E. Moser, F. Weisso, and M. Gra, “letters to nature,” vol. 395, no. October, pp. 583–585, 1998.

[38] K. D. Benkstein, N. Kopidakis, J. van de Lagemaat, and a. J. Frank, “Influence of the Percolation Network Geometry on Electron Transport in Dye-Sensitized Titanium Dioxide Solar Cells,” *J. Phys. Chem. B*, vol. 107, no. 31, pp. 7759–7767, Aug. 2003.

[39] N. R. Neale, N. Kopidakis, J. van de Lagemaat, M. Grätzel, and A. J. Frank, “Effect of a coadsorbent on the performance of dye-sensitized TiO2 solar cells: shielding versus band-edge movement.,” *J. Phys. Chem. B*, vol. 109, no. 49, pp. 23183–9, Dec. 2005.

[40] M. E. Gimon-Kinsel and K. J. Balkus, “Pulsed laser deposition of mesoporous niobium oxide thin films and application as chemical sensors,” *Microporous Mesoporous Mater.*, vol. 28, no. 1, pp. 113–123, Mar. 1999.

[41] J. Datka, “Acidic properties of supported niobium oxide catalysts: An infrared spectroscopy investigation,” *J. Catal.*, vol. 135, no. 1, pp. 186–199, May 1992.

[42] F. Lai, M. Li, H. Wang, H. Hu, X. Wang, J. G. Hou, Y. Song, and Y. Jiang, “Optical scattering characteristic of annealed niobium oxide films,” *Thin Solid Films*, vol. 488, no. 1–2, pp. 314–320, Sep. 2005.

[43] N. Ozer, T. Barreto, T. Biiyiiklimanli, and C. M. Lampert, “Characterization of sol-gel deposited niobium pentoxide films for electrochromic devices,” vol. 36, pp. 433–443, 1995.

[44] T. Nakajima and N. Watanabe, “STRUCTURAL RECHARGEABLE CHANGES OF Nb205 AND CATHODES FOR LITHIUM Vz05 AS,” pp. 17–22.

[45] K. Sayama, H. Sugihara, and H. Arakawa, “Photoelectrochemical Properties of a Porous Nb 2 O 5 Electrode Sensitized by a Ruthenium Dye,” vol. 100, no. 6, pp. 3825–3832, 1998.

[46] R. Ulrich, A. Du Chesne, M. Templin, and U. Wiesner, “Nano-objects with Controlled Shape, Size, and Composition from Block Copolymer Mesophases,” *Adv. Mater.*, vol. 11, no. 2, pp. 141–146, Feb. 1999.

[47] A. C. Finnefrock, R. Ulrich, G. E. S. Toombes, S. M. Gruner, U. Wiesner, C. Hall, and N. York, “The Plumber ’ s Nightmare : 1 A New Morphology in Block Copolymer - Ceramic Nanocomposites and Mesoporous Aluminosilicates,” pp. 13084–13093, 2003.

[48] D. Zhao, “Triblock Copolymer Syntheses of Mesoporous Silica with Periodic 50 to 300 Angstrom Pores,” *Science (80-.).*, vol. 279, no. 5350, pp. 548–552, Jan. 1998.

[49] K. M. Coakley and M. D. McGehee, “Photovoltaic cells made from conjugated polymers infiltrated into mesoporous titania,” *Appl. Phys. Lett.*, vol. 83, no. 16, p. 3380, 2003.

[50] K. M. Coakley, Y. Liu, M. D. McGehee, K. L. Frindell, and G. D. Stucky, "Infiltrating Semiconducting Polymers into Self-Assembled Mesoporous Titania Films for Photovoltaic Applications," *Adv. Funct. Mater.*, vol. 13, no. 4, pp. 301–306, Apr. 2003.

[51] L. Kavan, M. K. Nazeeruddin, P. Liska, and M. Gra, "Organized Mesoporous TiO 2 Films Exhibiting Greatly Enhanced Performance in Dye-Sensitized Solar," vol. 70, pp. 7–10, 2005.

[52] M. Nedelcu, S. Guldin, M. C. Orilall, J. Lee, S. Hüttner, E. J. W. Crossland, S. C. Warren, C. Ducati, P. R. Laity, D. Eder, U. Wiesner, U. Steiner, and H. J. Snaith, "Monolithic route to efficient dye-sensitized solar cells employing diblock copolymers for mesoporous TiO2," *J. Mater. Chem.*, vol. 20, no. 7, p. 1261, 2010.

[53] M. Nedelcu, J. Lee, E. J. W. Crossland, S. C. Warren, M. C. Orilall, S. Guldin, S. Hüttner, C. Ducati, D. Eder, U. Wiesner, U. Steiner, and H. J. Snaith, "Block copolymer directed synthesis of mesoporous TiO2 for dye-sensitized solar cells," *Soft Matter*, vol. 5, no. 1, p. 134, 2009.

[54] P. Docampo, S. Guldin, M. Stefik, P. Tiwana, M. C. Orilall, S. Hüttner, H. Sai, U. Wiesner, U. Steiner, and H. J. Snaith, "Control of Solid-State Dye-Sensitized Solar Cell Performance by Block-Copolymer-Directed TiO2 Synthesis," *Adv. Funct. Mater.*, vol. 20, no. 11, pp. 1787–1796, Jun. 2010.

[55] T. H. Epps, E. W. Cochran, T. S. Bailey, R. S. Waletzko, C. M. Hardy, and F. S. Bates, "Ordered Network Phases in Linear Poly (isoprene- b -styrene- b - ethylene oxide) Triblock Copolymers," pp. 8325–8341, 2004.

[56] G. V Naik, J. L. Schroeder, T. D. Sands, and A. Boltasseva, "Titanium nitride as a plasmonic material for visible wavelengths."

[57] M. B. Cortie, J. Giddings, and a Dowd, "Optical properties and plasmon resonances of titanium nitride nanostructures.," *Nanotechnology*, vol. 21, no. 11, p. 115201, Mar. 2010.

[58] Z. Jacob, I. Smolyaninov, and E. Narimanov, "Broadband Purcell effect: Radiative decay engineering with metamaterials," vol. 2, no. 4, pp. 534–537, Oct. 2009.

[59] D. Slocum, S. Inampudi, D. C. Adams, S. Vangala, N. a. Kuhta, W. D. Goodhue, V. a. Podolskiy, and D. Wasserman, "Funneling Light Through a Subwavelength Aperture with Epsilon-Near-Zero Materials," vol. 1, no. 6, pp. 1090–1099, Mar. 2011.

[60] C. Delacour, B. Pannetier, J.-C. Villegier, and V. Bouchiat, "Quantum and thermal phase slips in superconducting niobium nitride (NbN) ultrathin crystalline nanowire: application to single photon detection.," *Nano Lett.*, vol. 12, no. 7, pp. 3501–6, Jul. 2012.

[61] R. Shipra, N. Kumar, and a. Sundaresan, "Surface ferromagnetism and superconducting properties of nanocrystalline niobium nitride," *Mater. Chem. Phys.*, vol. 139, no. 2–3, pp. 500–505, May 2013.

[62] M. Ziegler, L. Fritzsch, J. Day, S. Linzen, S. Anders, J. Toussaint, and H.-G. Meyer, "Superconducting niobium nitride thin films deposited by metal organic plasma-enhanced atomic layer deposition," *Supercond. Sci. Technol.*, vol. 26, no. 2, p. 025008, Feb. 2013.

[63] T. S. Bailey, H. D. Pham, and F. S. Bates, "Morphological Behavior Bridging the Symmetric AB and ABC States in the Poly (styrene- b -isoprene- b - ethylene oxide) Triblock Copolymer System," pp. 6994–7008, 2001.